SPECT detectors: the Anger Camera and beyond

2011 Phys. Med. Biol. 56 R145

(http://iopscience.iop.org/0031-9155/56/17/R01)

Phys. Med. Biol. **56** (2011) R145–R182 doi:10.1088/0031-9155/56/17/R01

TOPICAL REVIEW

SPECT detectors: the Anger Camera and beyond

Todd E Peterson[1] **and Lars R Furenlid**[2]

[1] Institute of Imaging Science, Department of Radiology and Radiological Sciences, Department of Physics, and Program in Chemical and Physical Biology, Vanderbilt University, Nashville, TN, USA
[2] Center for Gamma-Ray Imaging, Department of Radiology, and College of Optical Sciences, University of Arizona, Tucson, AZ, USA

E-mail: todd.e.peterson@vanderbilt.edu

Received 4 April 2011, in final form 28 June 2011
Published 9 August 2011
Online at stacks.iop.org/PMB/56/R145

Abstract
The development of radiation detectors capable of delivering spatial information about gamma-ray interactions was one of the key enabling technologies for nuclear medicine imaging and, eventually, single-photon emission computed tomography (SPECT). The continuous sodium iodide scintillator crystal coupled to an array of photomultiplier tubes, almost universally referred to as the Anger Camera after its inventor, has long been the dominant SPECT detector system. Nevertheless, many alternative materials and configurations have been investigated over the years. Technological advances as well as the emerging importance of specialized applications, such as cardiac and preclinical imaging, have spurred innovation such that alternatives to the Anger Camera are now part of commercial imaging systems. Increased computing power has made it practical to apply advanced signal processing and estimation schemes to make better use of the information contained in the detector signals. In this review we discuss the key performance properties of SPECT detectors and survey developments in both scintillator and semiconductor detectors and their readouts with an eye toward some of the practical issues at least in part responsible for the continuing prevalence of the Anger Camera in the clinic.

(Some figures in this article are in colour only in the electronic version)

Introduction

The field of nuclear medicine, one of the most sensitive methods for obtaining information on biological function for the purpose of medical diagnoses, precedes the development of image-forming radiation detectors by several decades (Patton 2000). The earliest studies utilized the *tracer principle* (Chiewitz and Hevesy 1935), the introduction of minute amounts of radioactive

material into a subject, in conjunction with external radiation detectors to study physiological processes, such as the velocity of blood flow (Blumgart and Yens 1927, Patton 2003). The first imaging applications relied upon a collimated counter that was scanned across the patient in steps to form a crude two-dimensional image of the radiotracer distribution (Cassen *et al* 1951). The emergence of the practical imaging of single-photon-emitting radionuclides, however, can be traced to the development of the sodium iodide (NaI(Tl)) scintillation camera by Hal Anger in the 1950s (Anger 1952). The basic design of a large-area NaI(Tl) scintillation crystal, read out by an array of photomultiplier tubes (PMTs), in combination with an absorptive collimator has been so influential that it is nearly universally referred to as the 'Anger Camera' (a name that likely has caused some confusion to newcomers to the field) and has formed the basis for the vast majority of clinical nuclear medicine imaging systems for many decades. The Anger Camera collimator, most often an array of parallel holes resembling an assembly of lead soda straws, constrains the angles of incidence by which the decay photons can enter the detector material. Using a detector that provides spatial information on individual photon interactions in combination with a parallel-hole collimator allows for the creation of two-dimensional projection images of the radiotracer distribution—an image formation process related to the 2D Radon transform (see section 17.1.4 of (Barrett and Myers 2004)). Planar imaging of this sort is sometimes referred to as scintigraphy—the bone scan being a common clinical example of this technique. Single-photon emission computed tomography (SPECT) involves reconstruction of three-dimensional radiotracer distributions from such two-dimensional projection images acquired at multiple angles. For a full discussion of image reconstruction and many other aspects of emission tomography, the reader is referred to Wernick and Aarsvold (2004).

The objective of this paper is to survey recent developments in SPECT detector technology, with particular attention paid to performance characteristics relative to the still prevalent Anger Camera. While alternative approaches to the Anger Camera have been explored throughout the last 50 years, in the last decade or so the pace of research has accelerated, and some new detector approaches have begun to gain traction in a number of applications. On the one hand, these developments have emerged from technological advances in detector materials, readout electronics and computing power. As important or more so, however, have been the opportunities offered by the emerging importance of some specific imaging applications, especially those with small fields of view relative to whole-body scanning (Madsen 2007).

Small-animal imaging has become a major research area over the last ten to fifteen years. The demand for *in vivo* imaging in the preclinical arena has grown rapidly with the development of animal models of human diseases, including transgenic mice. Preclinical imaging spans many modalities, but SPECT has emerged as a powerful tool (Meikle *et al* 2005, Franc *et al* 2008). The small size of rodent subjects necessitates spatial resolutions a factor of 10 or better than for human imaging if structures are to be visualized and quantified, while the sensitivity must be sufficient that good image quality can be achieved in a practical length of time (governed by animal welfare considerations) with a reasonable amount of activity administered (based on radiation dose to the subject and adherence to the tracer principle). These demands have spawned innovation in both collimation and detection. Beyond the desire to meet the unique demands of small-animal imaging, preclinical imaging is an attractive area in which to explore new detector technologies, as the small size of the subjects to be imaged means that real imaging can be performed using less detector material (and accompanying readout) than would be needed for human imaging applications. Preclinical imaging can be viewed as a useful testing ground for new detector technologies, although some strategies for small-animal imaging may not be feasible to scale up to clinical applications.

A clinical application that has motivated the development of new detector technologies recently is myocardial perfusion imaging. One reason that clinical SPECT systems have long

centered on the Anger Camera is because of the ability to conduct a wide array of imaging procedures, from planar renal and bone scans to SPECT studies of cerebral blood flow, using a general-purpose system. However, clinical nuclear medicine has evolved such that the majority of procedures are myocardial perfusion SPECT studies (rest–stress tests)—cardiac studies made up 57% of all nuclear medicine procedures in the United States in 2006 (Mettler *et al* 2009). The heavy demand for this one type of study coupled with the increasing presence of scanners within cardiology practices has created a market for specialized SPECT systems. Several companies now market dedicated cardiac imaging systems, including at least two that utilize CdZnTe pixel detectors (Volokh *et al* 2008, Gambhir *et al* 2009, Garcia *et al* 2011).

A third imaging task that has been the focus of innovation in detector technologies is scintimammography—also sometimes referred to as molecular breast imaging (O'Connor *et al* 2007) or breast-specific gamma imaging (Brem *et al* 2006). Planar scintimammography using ^{99m}Tc-Sestamibi potentially offers good sensitivity and specificity for the detection of malignancies, particularly for women with radio-opaque breasts for whom mammograms often are inconclusive. The large-area Anger Cameras in general-purpose clinical systems are limited in their ability to get close to the breast and can yield images in which the vast majority of the counts come from the heart and liver. Recent purpose-built breast imaging devices have improved upon scintimammography with an Anger Camera by adopting formats that allow the camera to be positioned closer to the breast in a geometry similar to that employed in x-ray mammography, although generally utilizing less compression (Pani *et al* 1997). The use of parallel-hole collimation with this configuration limits the number of counts arising from outside the breast. Cameras built specifically for breast imaging have been designed primarily to offer better spatial resolution than the Anger Camera to improve the detection of small lesions (Tsui *et al* 1978), although some attention has been paid to improving energy resolution as a means of obtaining better contrast through the use of narrower energy windows to reject scatter (Hruska and O'Connor 2006).

Additional applications driving interest in new detector technologies in single-photon imaging include brain imaging and pre- or intra-operative sentinel node detection. There has been a renewed interest over the last couple of years in alternative collimation schemes for brain imaging, with many of the concepts incorporating multiple, compact detectors in a manner similar to that previously proposed in the 1990s (Rogulski *et al* 1993). In some respects, these recent efforts also can be considered extensions of the methodologies exploited in small-animal imaging. Multi-pinhole (Goorden *et al* 2009), slit-slat (Mahmood *et al* 2009), and diverging (Ogawa and Muraishi 2010) collimators are under investigation, and the moderate field of view needed along with the need for good spatial resolution provides motivation to pair these collimators with new types of detectors. Meanwhile, intraoperative gamma cameras for sentinel lymph node detection need cover only a small field of view and compactness is desirable in a surgical suite. This combination of parameters has given rise to a variety of purpose-built intraoperative imaging devices (Kopelman *et al* 2005, Sanchez *et al* 2006, Tsuchimochi *et al* 2008, Vermeeren *et al* 2010).

One property of SPECT that is often touted, though as yet used only infrequently, is the possibility of imaging more than one radionuclide simultaneously. This so-called dual-isotope imaging requires sufficient energy resolution from the detector to separately identify the photopeaks from each radionuclide. One combination of radionuclides of particular interest for dual-isotope studies is ^{99m}Tc (140 keV) and ^{123}I (159 keV). The better the energy resolution is, the better the delineation of photopeaks will be. At least as important is the fact that better energy resolution allows for narrower energy windows to be set around each gamma-ray energy, reducing the number of down-scattered photons from higher energies that fall within the windows of lower-energy gamma rays. The rapid evolution of molecular

imaging is likely to lead to increased demand for dual-isotope imaging. For instance, choosing the proper molecularly-targeted cancer therapy, as well as early assessment of response to such therapy, may be aided through the assessment of more than one functional property of the target, such as the expression level of a particular gene and the extent of hypoxia. An example from the cardiovascular arena would be the colocation of a lipid plaque and an inflammatory response (Spagnoli *et al* 2007).

SPECT detector basics

Key properties

There are a small number of properties that characterize the usefulness of any imaging detector regardless of the particular application: SPECT, PET, gamma-ray astrophysics, or homeland security. The relative importance of the different aspects of performance and the optimal choice for each varies by application and specific imaging task (Barrett *et al* 1995a). Obviously, it is first paramount that any detector system has an acceptable efficiency for actually detecting the photons of interest. The density, effective atomic number and thickness are the key parameters that govern detection efficiency, and here the choice is heavily influenced by the energy of the photons to be detected. While maximizing the detection efficiency has the desirable effect of improving counting statistics, often there are trade-offs between efficiency and another of the desired properties, most frequently spatial resolution, that may impose a practical limit on the detection efficiency. The nature of these trade-offs is not always immediately obvious; Muehllehner showed that in emission tomography, as the spatial resolution is improved, fewer photons are required to achieve the same visual image quality (Muehllehner 1985). This observation suggests that in some cases it may be worth sacrificing detection efficiency for the sake of improved spatial resolution.

The formation of an image necessitates the encoding of spatial information at some stage of the detection process. There are a number of ways in which this can be accomplished. The original approach was to translate a single detector element across the desired field of view to build up an image piece by piece, as was done by the rectilinear scanner (Cassen *et al* 1951). Another method is to utilize arrays of single pixel detectors such that the spatial information follows from the distribution of counts across the elements. The most common approach in gamma-ray scintigraphy and SPECT, however, is to utilize a continuous detector that provides multiple signals that can be processed to yield estimates of spatial coordinates of individual gamma-ray interactions. As will be described in detail later, there are several different strategies for obtaining spatial information. While the spatial resolution is an important property of an imaging detector, it is not the only factor that determines the final image resolution. The collimator and reconstruction algorithm (for SPECT) also contribute, and consequently, conventional wisdom has been that there is little advantage to be gained by using a detector whose spatial resolution significantly exceeds that of its parallel-hole collimator. The prevalence of this view undoubtedly has contributed to the continuing dominance of the Anger Camera. With the adoption of iterative reconstruction algorithms that incorporate accurate forward models and thereby accomplish at least some resolution recovery, this is no longer an obvious point. This view is even less relevant when schemes other than parallel-hole collimation are employed, and as noted previously, the increasing use of pinholes and other types of collimators has contributed to interest in alternatives to the Anger Camera.

Energy resolution is another important consideration in a single-photon imaging detector system. If the magnitude of the signal emanating from a detector is proportional to the energy

deposited in it by an interacting gamma ray, a window on a histogram of signal amplitudes can be set to select photons of interest based on energy. This energy windowing allows for the removal from the image data of photons that have lost energy via Compton scattering in the subject or the collimator, as well as any characteristic x-rays created within the collimator material. The better the energy resolution offered by a detector, the narrower the energy window that can be used, thereby reducing the number of unwanted photons making it into the image data. As mentioned above, a further opportunity offered by the energy discriminating capabilities of a detector is the possibility of simultaneously imaging the distribution of more than one radionuclide, creating separate images for each by sorting the photon interactions within the detector into individual energy windows. Here the benefit of good energy resolution comes not only from the ability to discriminate the individual full-energy peaks from each radionuclide through the use of narrow energy windows, but also through the reduction of contamination in the energy window for one radionuclide by down-scattered photons from the higher energy gamma-ray emissions of another radionuclide (Links 1996). While schemes for crosstalk and scatter compensation in dual-isotope studies have been developed (Ichihara *et al* 1993, El Fakhri *et al* 2001), improvements in energy resolution should result in improved quantitative capabilities.

While detection efficiency, spatial resolution and energy resolution are arguably the three most important characteristics of a SPECT detector, there are several other properties that need also be considered. It is highly desirable for a detector to exhibit good uniformity: that the detection efficiency, spatial resolution and energy resolution do not vary substantially depending on where the photon interacted within the detector. While it is possible to apply corrections to the data to compensate for spatial variations in detector response, such as division by flood images, doing so requires not only that the non-uniformities be sufficiently well characterized, but also that the detector performance be stable over time (Rogers *et al* 1982). The application of uniformity corrections also generally will alter the statistics of the data, which may have started out with true Poisson counting statistics, but at best become scaled Poissons following correction. Stability over time obviously is important even in the absence of spatial non-uniformities and can be thought of as uniformity in the time domain. Maintaining stable performance over time requires a high degree of stability from all power and bias supplies.

Some other important qualities of detector systems for single-photon imaging applications include count-rate capability, mechanical robustness and cost. Count-rate demands typically are not as high in single-photon imaging as in positron-emission tomography (PET), as the collimator limits the sensitivity, and considerations such as radiation dose and mass effects (Kung and Kung 2005) often restrict the amount of injected activity. Nevertheless, the count-rate capability must be sufficient (>5 kcps) to allow image (and calibration) data to be collected within a reasonable time. One way to enhance the count-rate capability of a SPECT system is to deploy multiple modular detectors with independent readouts, either as separate cameras (Milster *et al* 1990) or as components making up a larger camera (Eisen *et al* 1996).

Additionally, SPECT detectors need to be physically robust enough to operate in any orientation in the gravity field. Since a stationary imaging subject is the ideal experimental condition, most conventional SPECT systems require one or more cameras to rotate about the subject to collect complete projection data sets. The same consideration applies to stationary systems with a ring of cameras, where detectors are permanently mounted in a variety of orientations. Cameras also need to be stable against temperature changes in ambient air, be resistant to microphonics from building vibrations, and have long-lasting hermetic seals or other dry-environment strategies if there are any moisture-sensitive components.

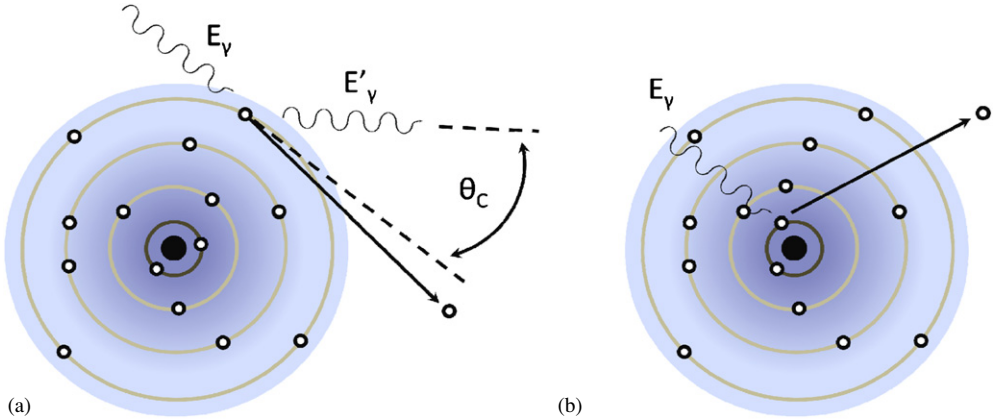

Figure 1. (a) Schematic representation of the Compton–scatter interaction in which a gamma-ray photon transfers part of its energy to an outer-shell electron ($E_\gamma > E_\gamma'$). (b) Schematic representation of a photoelectric interaction in which a gamma ray transfers all of its energy to the binding energy and residual kinetic energy of a core electron.

For any detection scheme to achieve widespread use it must not cost significantly more to manufacture than competing approaches with similar performance. The proper way to compare the cost of different detectors is to consider the full system including all electronics. While the detector volume or imaging surface area may seem like appropriate metrics for cost comparison, a fairer basis is the cost per unit of space-bandwidth product. The space-bandwidth product is given by the area of the detector divided by the area of the detector's point-spread function (PSF) (Ozaktas and Urey 1993, Barrett and Hunter 2005), and is thus a way to characterize the number of independent locations to which a detector can assign events. The underlying assumption in this formulation is that a properly designed system should employ a collimation scheme that fully exploits the available space-bandwidth product of the detector system. One simple example of this principle is pinhole SPECT. Few alternatives to the Anger Camera match it in area, but a detector with a narrower PSF can be operated at a smaller pinhole magnification to achieve the same image resolution as the Anger Camera, so it need not necessarily be as large.

Building blocks

As will be described later, there are many different approaches to making a detector system for planar nuclear imaging or SPECT. Regardless of the approach, the objective is to convert the gamma-ray photon's energy into an electrical signal. The limiting factor in the performance of a well-designed system is the number of information carriers at the point of conversion to an electrical signal. These information carriers are in the form of scintillation photons, electron–hole pairs, or electron–ion pairs depending on the detector technology. There are a few fundamental building blocks common to any such system; the differences between competing approaches being in the choice of how to implement each block.

The first building block is the converter: the piece of the system in which the *emitted* gamma-ray photon interacts and deposits energy. When a gamma ray interacts in a material, there are two principal possible interactions as depicted in figure 1, photoelectric absorption and Compton scatter. In photoelectric absorption, the gamma-ray photon excites a core

electron of one of the atomic constituents of the detector material with the gamma-ray energy dividing between the binding energy of the core electron before excitation and its kinetic energy as it propagates after excitation. The gamma-ray energy lost to the binding energy is left in the form of an empty core hole that relaxes and contributes to the signal via the emission (and reabsorption) of a secondary x-ray, a cascade of Auger electrons, excitation of vibrations, or combinations thereof. In Compton scatter, the gamma-ray interacts with a loosely bound electron and deflects from its original path, in the process conveying some of its energy and momentum to the electron. Both the Compton-scattered photon and resulting electron continue to propagate and undergo further interactions in the converter material.

If the energy of the gamma-ray photon is above 1.1 MeV, which is rare for SPECT, a third interaction becomes possible, namely the conversion of the photon into an electron and positron in a process known as pair production. Within the 30–250 keV energy range of most SPECT studies, the energy deposition generally occurs in a cascade with zero, one, or two Compton scatters followed by one terminal photoelectric absorption. However, there are a number of mechanisms by which less than the total gamma-ray energy can be deposited in the converter. Among the most common are Compton-escape, where either the scattered gamma ray or the Compton electron leaves the converter material, and escape of the secondary x-ray following photoelectric absorption. These losses are more likely to occur when the gamma ray interacts close to one of the faces of the detector material.

When the converter is a condensed-phase material with a periodic structure that creates an electronic band structure, the movement of a primary electron through the lattice of the detector material creates time-varying electric fields that couple efficiently to valence-band electrons, exciting them across the bandgap to form ensembles of electron–hole pairs as it loses energy, as illustrated in figure 2. In an ideal scenario, the number of electron–hole pairs created is simply the energy of the gamma-ray photon divided by the bandgap. In practice the average energy cost per signal-inducing electron–hole pair is higher than the bandgap energy due to recombination as well as other processes by which the primary electron loses energy.

The most common gamma-ray converter choice is a scintillator, which converts gamma-ray energy deposited in the detector into a burst of optical (or near-optical) photons as electron–hole pairs recombine at luminescent sites intentionally introduced as dopants. A second stage then converts these optical photons into an electrical signal, with PMTs being the most common way to accomplish this. Scintillator materials are typically inorganic salts such as sodium iodide or cesium iodide that are doped with traces ($\sim$0.1 mole%) of rare-earth elements such as thallium or cerium. They may comprise single large crystals or an ensemble of smaller crystallites, but in either case have periodic lattices that give rise to an electronic band structure and a bandgap. As discussed below, the production and detection of the scintillation photons involves a number of random processes such that the raw light-sensor output as a function of gamma-ray photon energy and interaction location is generally a random variable that ideally follows or approaches Poisson statistics.

The chief alternative to scintillators is to use a detector material in which the gamma-ray energy is converted into electrical charge that is read out directly. Semiconductor materials achieve this when the absorbed energy creates an ensemble of electron–hole pairs, via physics processes entirely analogous to what happens in scintillators, that are made to drift in opposite directions by application of an electric field. These moving charges then induce signals on electrodes (Shockley 1938, Ramo 1939). There are random effects that affect the signals in semiconductors as well, including the trapping of the holes or electrons in crystal defects and losses to other excitations in the crystal, but in general the ratio of the signal variances to the

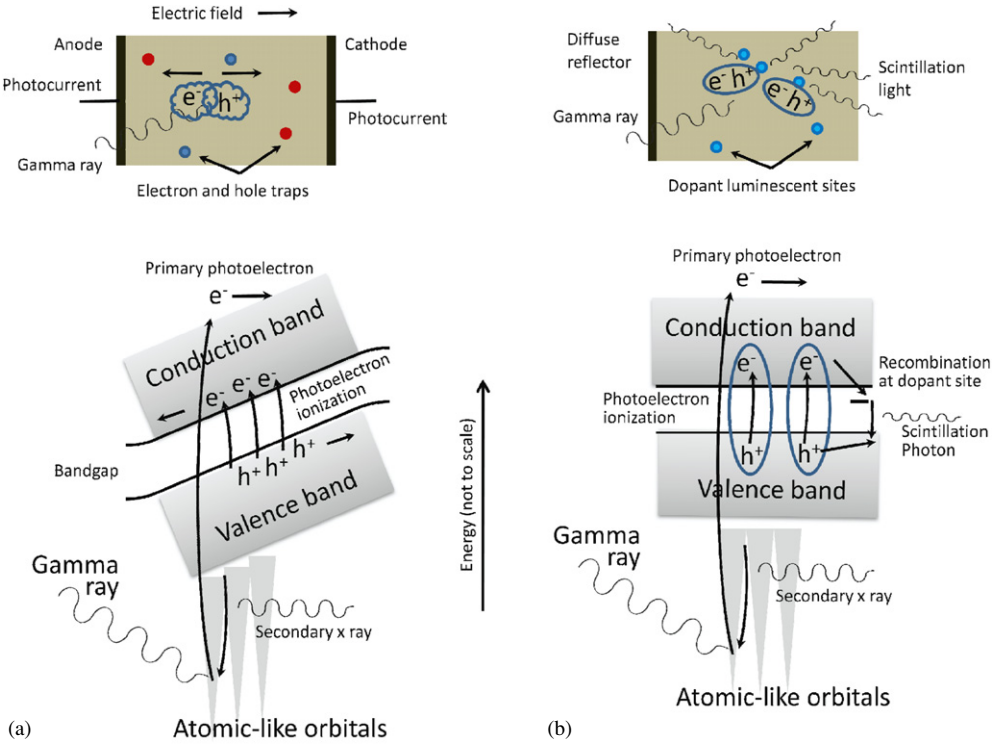

Figure 2. (a) Representation of the photoelectric process in a direct-conversion material, showing the excitation of electron–hole pairs that drift in opposite directions under the influence of an externally applied electric field. The moving charge induces electrical signals on the electrodes that can be read out. (b) Photoelectric interaction in a scintillator also creates electron–hole pairs, but in the absence of the applied field they stay together as loosely bound pseudoparticles known as excitons. The excitons diffuse to luminescent centers where they recombine, emitting secondary scintillation photons in the process that can be read out using an appropriate light sensor.

signal means (the Fano factor as discussed later) are much smaller for semiconductors than other types of gamma-ray converters.

Gas-based detectors work in a similar manner by converting the absorbed energy into a cloud of electron–ion pairs that drift toward signal electrodes. Although several different configurations have been investigated (Bolozdynya *et al* 1997, Tsyganov *et al* 2008, Azevedo *et al* 2011), gas-based detectors have not found widespread use in SPECT and will not be discussed further.

Once the deposited photon energy is converted to electrical charge, the next building block required is some form of readout electronics. While the ultimate aim of this electronics chain is to digitize information for further processing within a computer, often there are amplification, shaping, and logic steps that precede this digitization. The electronics implementation can vary widely depending on the choice and physical layout of the detector, and whether there is an inherent gain process in the sensor, such as dynode stages in a PMT or avalanche multiplication in a photodiode.

To arrive at final certification of a photon interaction as an event of interest for image formation requires some amount of additional evaluation. Because of the statistical nature of the signal-generation process itself, these evaluations necessarily involve estimation, which we

identify as another of the important building blocks. The key properties to be estimated are the energy of the incident photon and the interaction location in two, or possibly three, dimensions. Estimation of these parameters can be carried out with varying levels of sophistication and implemented at different stages of the imaging chain, from the initial signal readout to a post-processing step in the computer after all data have been collected. While it may be convenient to quickly estimate event attributes with *ad hoc* combinations of signals, there is virtually always a performance advantage in applying a rigorous statistical estimation method (Barrett *et al* 2009).

Anger Camera

As previously mentioned, the primary detection strategy for single-photon imaging in biomedical applications for more than 50 years has been based on the gamma camera design of Hal Anger (Anger 1952). To properly appreciate the more recent developments in SPECT detectors, it is helpful to examine the reasons for the ubiquity of the Anger Camera. The basic design of gamma cameras of this type consists of a large-area, continuous NaI(Tl) scintillator crystal coupled to an array of PMTs (generally with a light guide between the crystal and the PMTs), as shown in figure 3. Anger's original camera consisted of a $\frac{1}{4}''$ thick NaI(Tl) crystal that was $5''$ in diameter and coupled to seven PMTs (Anger 1952). Information on the energy deposited by a photon interaction is obtained by summing the signal amplitudes of all PMTs, while spatial information is extracted based on linear combinations of the distribution of signals across the array of PMTs.

NaI(Tl) was among the first scintillators developed (Hofstadter 1949), yet it remains a nearly ideal scintillator for detection of the 140 keV gamma rays emitted in the decay of ^{99m}Tc, the most widely used radionuclide for SPECT. The attenuation coefficient at 140 keV (2.64 cm^{-1}) is sufficient to achieve good detection efficiency with a relatively thin crystal—94% total efficiency in a $\frac{1}{2}''$ crystal. NaI(Tl) also has a high light output, meaning that a large number of optical photons are created for each keV of energy deposited in the scintillator ($\sim$40 photons/keV), which is important for both the energy and spatial resolution. Another key factor in the preeminence of the Anger Camera is the fact that NaI(Tl) can be grown as very large crystals (up to $\sim$80 cm in diameter), allowing detectors to be fashioned from a single crystal with sufficient size for body-imaging applications. The scintillation light rise time is fast, and the decay time is relatively short such that count rates on the order of 10^5 per second are possible.

The PMTs in an Anger Camera are positioned in a close-packed, hexagonal array and coupled to a fused-quartz light guide via index-of-refraction-matching optical grease or room-temperature-vulcanizing (RTV) silicone. The number of optical photons created following a gamma-ray interaction is generally proportional to the energy deposited (Dorenbos *et al* 1995), and these photons are emitted isotropically from their point of creation. The PMT closest to the point of interaction, because it subtends the largest solid angle with respect to that point, will collect the largest number of optical photons. Consequently, it will have the largest output signal, with the signal output of the other PMTs decreasing in amplitude with increasing distance from the interaction point. The location of the gamma-ray interaction therefore can be estimated based on the distribution of signal amplitudes in the PMTs. Anger's original process for decoding the interaction position involves calculating the centroid of the position-weighted PMT outputs, a process often referred to as Anger Logic or Anger Arithmetic (Anger 1958), although there are several ways in which it is carried out. The simplest method is to tie the outputs of the PMTs to the nodes of a 2D resistor array such that four signals are derived, representing a division of the total charge collected on the PMT anodes in four directions

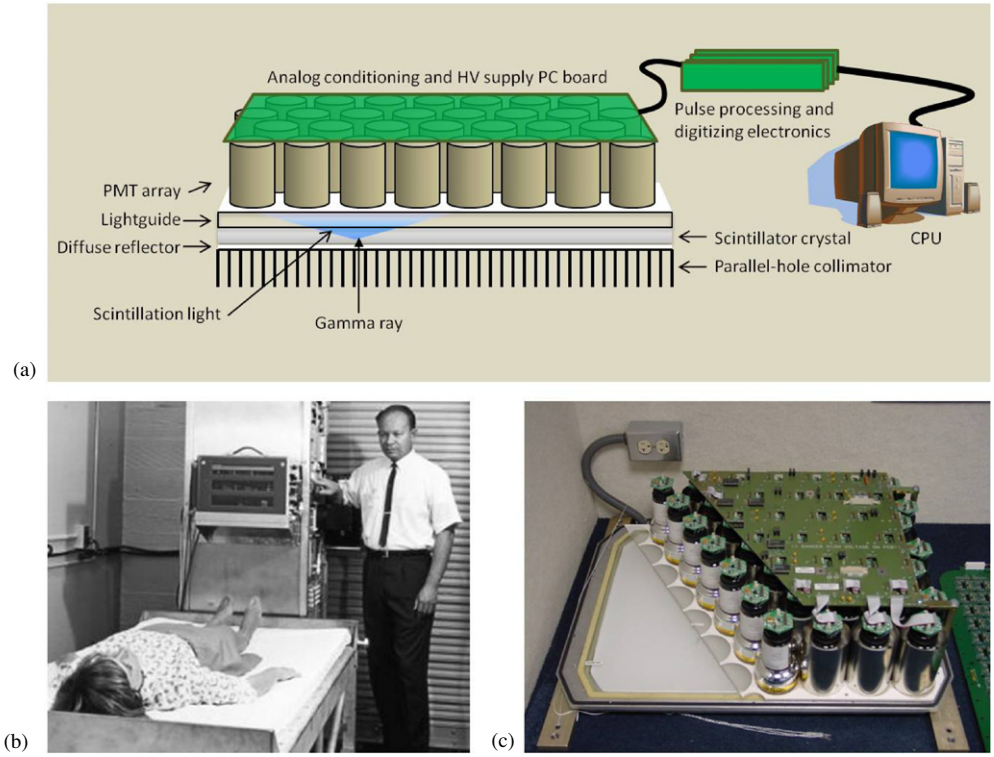

Figure 3. (a) The basic structure of the Anger Camera comprises a collimator, a monolithic scintillator crystal, a light guide that allows light to spread and an array of PMTs with related electronics. Position estimation was originally performed with analog circuitry; in current systems PMT outputs are digitized and all processing is digital. (b) Hal Anger shown with early example of his camera being applied in a clinical setting (reprinted by permission of the Society of Nuclear Medicine from: Nuclear Medicine Pioneer, Hal O Anger, 1920–2005. J. Nucl. Med. Technol. 2005; 33(4): 250–3). (c) A cutaway of an actual camera (courtesy of M Wernick and J Aarsvold).

that can be combined as differences normalized by sums to give direct position values. In other variants of the Anger Camera, each PMT has its own A/D converter and the Anger arithmetic is carried out in software, allowing the application of various weighting schemes. Equation (1) shows a fairly general form for this type of processing. The position estimates are computed by combining only the PMTs at known locations x_i,y_i that have signals S_i that exceed a threshold $S_{\min}$. In the simple center of gravity calculation, the functions w return just the raw signals S_i:

$$\hat{x} = \frac{\sum_{S_i \geqslant S_{\min}} x_i w(x_i, S_i)}{\sum_{S_i \geqslant S_{\min}} w(x_i, S_i)}, \qquad \hat{y} = \frac{\sum_{S_i \geqslant S_{\min}} y_i w(y_i, S_i)}{\sum_{S_i \geqslant S_{\min}} w(y_i, S_i)}. \tag{1}$$

In practice all estimation schemes based on linear combinations of signals exhibit bias, i.e. errors in the event positioning, that can be seen as clustering of events preferentially under the footprints of the individual PMTs with fewer events in the regions between the PMTs. These spatial distortions, which have a characteristic pincushion shape visible in figure 4, typically are compensated for by applying a heuristic linearity correction that is derived from images of shadow masks that create a regular pattern of parallel lines or points on the camera face. A more sophisticated approach is to apply maximum-likelihood (ML) estimation methods to the

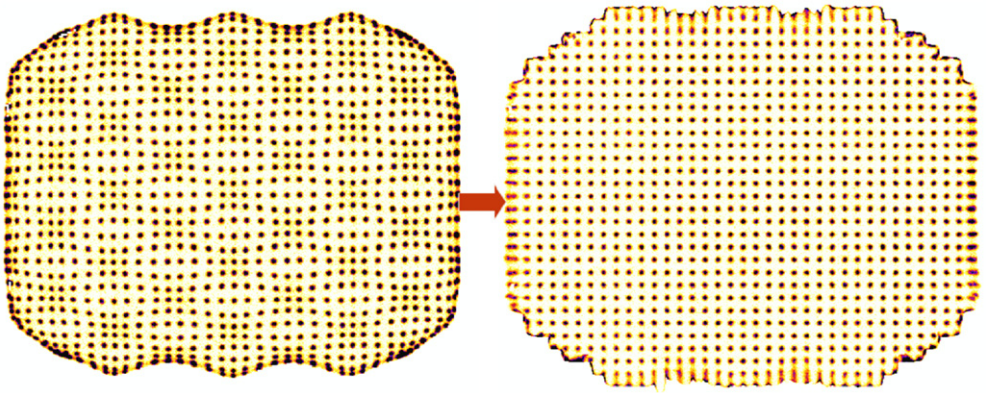

Figure 4. Positioning results from a regular array of points projected on the face of an Anger Camera before (left) and after (right) processing to correct for systematic distortions characteristic of Anger Arithmetic. From Villena *et al* (2010), © 2010 IEEE.

problem of position and energy estimation (Barrett *et al* 2009). The ML approach has distinct advantages, including being asymptotically unbiased and permitting position estimation out to the edge of the camera face (Milster *et al* 1990). ML methods will be discussed further later.

Typical performance values for present-day Anger Cameras are ∼10% full-width at half maximum (FWHM) energy resolution for ^{99m}Tc and ∼2–4 mm FWHM spatial resolution on an active camera face area of 21″ × 18″. A camera can typically support event rates up to 10^5 per second. Cameras require daily quality-assurance checks, usually incorporating at least measurement of a flood source in order to trim out drifts in PMT channel gains. Cameras last for many years, if not decades, especially if well sealed to prevent scintillation crystal yellowing.

The Anger Camera is a mature, cost-effective technology. The challenge for anyone wanting to develop a new detector scheme for SPECT or other single-photon imaging applications is to exceed one or more of the Anger Camera's performance parameters without severely compromising the others. In the following sections we discuss the main categories of detector materials and associated readout that have been applied to SPECT.

Advances in scintillators

Scintillators are the predominant material for the gamma-ray converter in imaging detector systems, with NaI(Tl) long having been the most common choice. Although a full description of scintillation involves several processes, a simple model is that electron–hole pairs created in scintillators stay bound to each other as mobile pseudoparticles known as excitons. Excitons eventually find their way to luminescent (dopant) centers where they can re-combine via radiative transitions with energies lower than the bandgap, emitting light in the process that, importantly, is at a wavelength that is not reabsorbed by the crystal. In many scintillators this recombination can proceed through different intermediate excited states, leading these scintillators to exhibit 'fast' and 'slow' components in their light emissions (Belyavskii *et al* 1971). The light output of a scintillator, given in terms of the number of optical photons produced per keV of energy deposited (photons/keV), ultimately governs both the

energy and spatial resolutions that can be achieved. In particular, it is the statistical variation in the number of optical photons produced for a given energy deposition that sets the limits on energy and position resolution, so high light output is desirable as it results in a higher signal-to-noise ratio.

Other critical factors characterizing scintillator performance are proportionality and the timing characteristics of the scintillation light output. In principle, the mean number of scintillation photons should be strictly proportional to the energy of the absorbed gamma ray, and deviation from this ideal relationship is termed non-proportionality. Recent advances in understanding this phenomenon focus on variations in the local exciton density, as caused by a material-specific secondary ionization pattern as a function of primary electron energy, and thereby a varying probability of exciton–exciton annihilation (Cherepy *et al* 2009, Payne *et al* 2009). A consequence is that an event in which an incident gamma ray undergoes a photoelectric interaction immediately will result in a different amount of light than one in which the gamma ray first undergoes a Compton scattering and then a photoelectric interaction of the secondary photon, even if the total gamma ray energy deposited is the same.

Another key property of a useful scintillator is that the wavelength of the optical photons be well matched to the absorption characteristics of the PMT photocathode or other light sensor. For the purposes of overall detection efficiency, high density in a scintillator is an advantage so as to provide a high interaction probability for the incident photons. However, it is preferable to have the photoelectric effect be as large a fraction of the total absorption cross-section as possible since both energy and spatial resolution benefit from localized energy deposition. If the first interaction of an incident photon is via Compton scattering, the resulting secondary photon may travel a significant distance in the crystal before undergoing a photoelectric interaction. In this case the energy deposition will be dispersed spatially and thus limit the ability to estimate the interaction point of the incident photon unless the readout is able to separately identify the two interactions. The photoelectric interaction probability scales roughly as Z^4, so high effective atomic number is highly desirable in any radiation detector (Reddy *et al* 1992).

The art of manufacturing scintillator-based cameras also involves treatments of scintillator entrance faces and edges to try to recover scintillation light initially emitted in directions away from the PMTs while at the same time creating well-behaved position-dependent response curves. The entrance-face reflectors are generally made Lambertian in character and contribute to smooth light spread over multiple PMTs. The edge treatments, which extend along the light guide as well as the scintillator crystal, can be either reflective to maximize the total light detected, and thereby the energy resolution, or absorptive to maximize the spatial resolution that can be achieved at the edge of the camera. Retro-reflective materials have been applied as alternative surface treatments for the entrance face (McElroy *et al* 2002, Heemskerk *et al* 2009). Much like a bicycle reflector or road sign, these retro-reflectors are designed to bounce light back at 180° to the incident ray, increasing the amount of light reaching the readout without significantly broadening the light spread.

While the continuous crystal read out by multiple PMTs has been the dominant design among scintillator-based imaging detectors, several other configurations have also been employed. One method is to construct an array of small, individual scintillator crystals (Truman *et al* 1994, Blazek *et al* 1995, Weisenberger *et al* 1998, 2001, Williams *et al* 2000) like the one shown in figure 5, typically with some form of reflective material filling the gaps between crystals in an effort to confine the scintillation photons to the individual crystal in which they are created. This approach is similar to the scintillator array design used in some PET detectors (Wong 1993, Cherry *et al* 1996). In a continuous crystal design the estimation of the position of interaction relies on the dispersion of optical photons leading to the generation

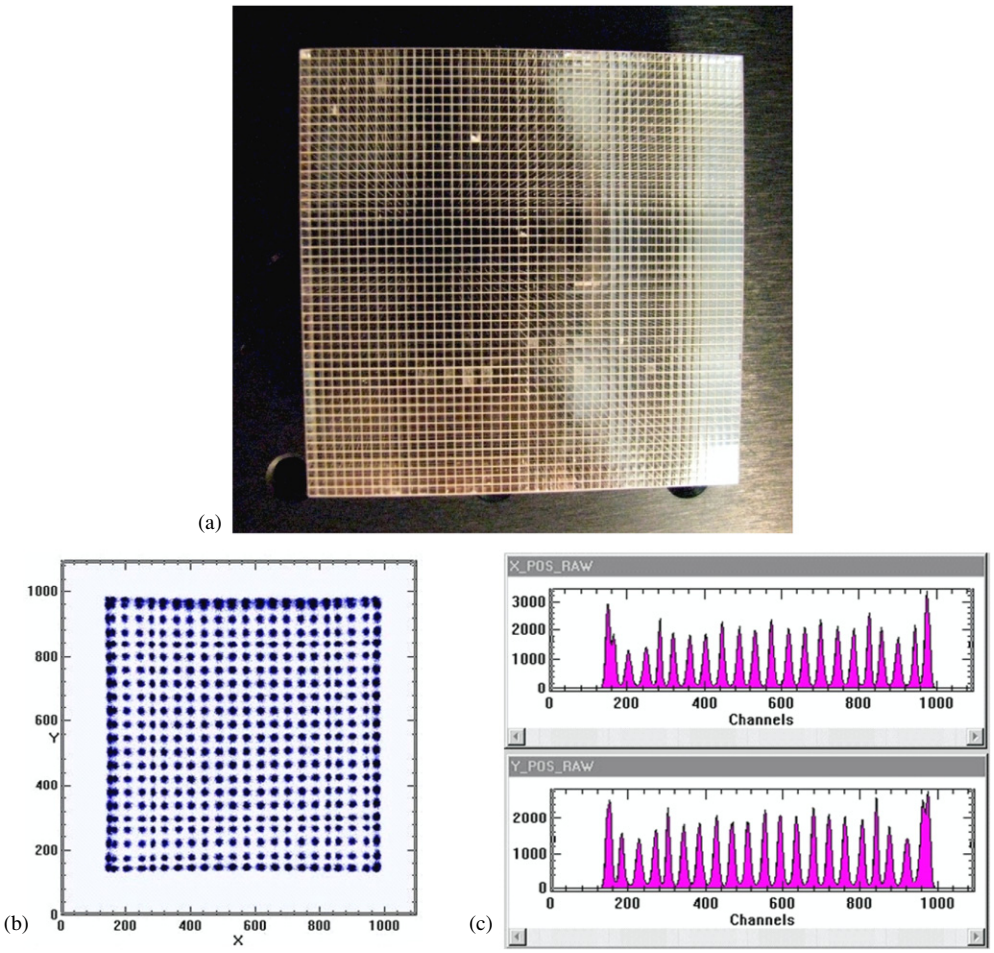

Figure 5. (a) A 48 × 48 scintillator array with 1 mm pitch. (b) Raw image from resistive-readout of a Burle Planacon MA-PMT coupled to a NaI(Tl) scintillator array. (c) *X* and *Y* projections of the 2D image shown in (b). (Photo courtesy of A Weisenberger, Jefferson Lab, while (b) and (c) are from Popov *et al* (2003), © 2003 IEEE.)

of signals in multiple PMTs. In contrast, in the scintillator-array approach the objective is to minimize the area over which the scintillation light is dispersed and then identify in which crystal the interaction occurred, a process referred to as decoding. The cross-sectional area of the individual crystals represents the fundamental limit to the potential spatial resolution, but besides the technical limitations to manufacturing and assembling small crystals, trade-offs in other aspects of detector performance impact the choice of crystal size. As the size of the crystal is decreased, energy resolution typically suffers due to decreased transmission efficiency of the scintillation photons as they undergo multiple reflections along the crystal elements. The unavoidable gaps between the crystals also reduce the total detection efficiency, and for a given total detector area, smaller crystal sizes mean more gaps and, therefore, less total detector material. Further, spatial resolution can be compromised as a result of Compton scattering giving rise to events in which scintillation photons are created in multiple crystals by a single incident gamma ray. While the lateral dimensions of the crystals used in scintillator

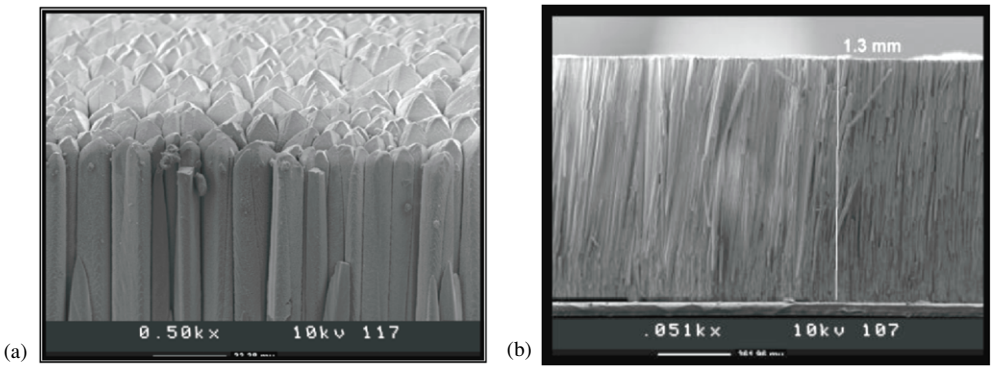

Figure 6. (a) Top and (b) cross-sectional SEM micrographs of a 1.3-mm-thick microcolumnar CsI(Tl) film. (Courtesy of V Nagarkar, RMD, Inc.)

arrays for single-photon applications typically have been in the 1–2 mm range (Bradley *et al* 2006, Xi *et al* 2010), PET detector modules with 0.5 mm crystals have been tested (St James *et al* 2009), with efforts underway to employ crystals of even smaller sizes. The quality of a segmented-crystal camera is judged by how well the crystals are resolved, which can be assessed from the peak-to-valley ratio of a line profile through a flood image like the ones shown in figure 5.

Another approach to scintillator-based imaging detectors is to utilize so-called micro-columnar crystal arrays like those shown in figure 6, typically CsI(Tl) (Nagarkar *et al* 1998, 2006, Tornai *et al* 2001). These detectors consist of needle-like crystals that are grown together. The small size of the individual crystals (down to $\sim$10 μm) can provide good intrinsic spatial resolution, as they provide a natural means of channeling the scintillation light, but the thickness of such arrays has been limited ($\leqslant$3 mm), such that to date they have found use primarily in low-energy gamma-ray and x-ray applications.

Several other scintillator configurations have been employed for imaging detector systems. One unique approach utilized an annular detector cut from a single NaI(Tl) crystal (Genna and Smith 1988). By surrounding the object to be imaged with detector material, only the imaging apertures need to rotate instead of the entire detector assembly. The increased detector volume leads to reduced mechanical complexity. More recently, Korevaar, Heemskerk, and Beekman developed a scintillator for use with a pinhole collimator in which the detector surface has a convex shape, constraining the angle of incidence of photons to near-normal incidence (Korevaar *et al* 2009a). Optical fibers with a limited numerical aperture are coupled normal to the curved crystal surface, restricting the range of incidence angles over which optical photons are transmitted. This scintillator–fiber bundle combination reduces the depth-of-interaction effects that can degrade spatial resolution in pinhole SPECT.

Table 1 lists the properties of the most common scintillator materials that have been used to create imaging detectors. NaI(Tl) remains the most widely used, largely because of its high light output and because it is possible to reliably grow large crystals, making it cost effective. While the hygroscopic property exhibited by NaI(Tl) is an undesirable trait in a scintillator, sufficient experience with packaging has developed over the many decades that it has been used that it does not constitute a significant disadvantage. CsI(Tl) in various forms has been used by a number of investigators (Gruber *et al* 1998, Tornai *et al* 2001, Despres *et al* 2006), and $YAlO_3$(Ce), better known as YAP, has also found use, most notably in the YAP-(S)PET small-animal scanner (Del Guerra *et al* 2006). More recently, there has been

Table 1. Some relevant properties of the most commonly used scintillators for SPECT. Data compiled from van Eijk (2002) and Barrett and Hunter (2005).

	Density ($g\ cm^{-3}$)	Attenuation at 140 keV (cm^{-1})	Max. emission (nm)	Decay time (ns)	Light yield (photons/keV)
NaI(Tl)	3.67	3.12	415	230	38
CsI(Tl)	4.51	4.53	540	680 (63%), 3340 (37%)	65
$LaCl_3$(Ce)	3.86	2.82	330	20 (70%), 213 (30%)	49
$LaBr_3$(Ce)	5.30	3.42	358	35 (90%)	61
$YAlO_3$(Ce)	5.50	1.81	350	30	21

considerable excitement surrounding lanthanum bromide (most commonly $LaBr_3$(Ce)) (Shah *et al* 2003) and lanthanum chloride ($LaCl_3$) (van Loef *et al* 2001) scintillators of various types, owing to their high light output and, consequently, their improved energy resolution (∼6% at 140 keV (Pani *et al* 2006)) in comparison to other scintillators. While the size of the crystals grown to date have been small in comparison to NaI(Tl), a number of investigators have made measurements with small LaBr-based imaging detectors (Despres *et al* 2006, Russo *et al* 2009).

It is worth noting that LSO, currently one of the more popular scintillators for PET detectors, and other scintillators containing lutetium are not well suited for SPECT applications due to the 2.6% natural abundance of radioactive ^{176}Lu. This intrinsic activity creates a background count rate of approximately 240 cps per cc of LSO (Melcher and Schweitzer 1992, Huber *et al* 2002). Whereas the coincidence requirement for PET effectively rejects most of this background except for a contribution to the random coincidence rate, the presence of this intrinsic activity has the potential to create unwanted counts for single-photon applications. While many of these background counts would likely be rejected by the application of an energy window, they would still contribute to the dead time, contributing 10s of kHz in even a modest sized gamma camera. In spite of this, the group at SUNY-Buffalo has created a background-subtraction scheme to facilitate SPECT studies on an LSO-based small-animal PET scanner (Rutao *et al* 2008).

Advances in scintillator readouts

As will be seen below, there are several options for converting the optical photons generated in scintillators into an electrical signal. The most important property for this stage of the detector chain is the quantum efficiency—the ratio of the number of photo-generated electrons to the number of incident scintillation photons. Since different scintillators have different emission spectra, the spectral response of the converter should be well matched to that of the scintillator to maximize the overall quantum efficiency.

The PMT, comprising an evacuated glass package with a photocathode light-to-electron converter followed by a string of electron-multiplying dynode stages, has long been the dominant method for converting optical photons to an electrical signal for all types of scintillator-based detector systems. The high amplification gain ($>10^6$) afforded by multi-stage PMTs minimizes the impact of noise in the rest of the electronic readout chain. PMTs have some disadvantages, including gain drift and eventual photocathode fatigue (Marshall *et al* 1947). Furthermore, most PMTs to date have a relatively low quantum efficiency (∼25%), which means that most of the scintillation light does not generate electrical signal. In the past several years, PMT manufacturers have roughly doubled the quantum efficiency

through a combination of improvements in photocathodes and the optical properties of the PMT package (Kapusta *et al* 2007).

Another practical drawback of PMT-based readouts of the kind used in the Anger Camera is that their bulky size limits the attainable intrinsic spatial resolution. Estimation of the gamma-ray interaction positions to better than the size of a single PMT requires that optical photons be incident upon multiple PMTs in a position-dependent manner. Using PMTs with a smaller entrance face can lead to better spatial resolution, but the larger number of PMTs required to cover the detector surface then drives up the cost and increases the number of channels of readout electronics.

In the past 25 years new PMT configurations have been developed that allow for new approaches to position estimation in scintillation cameras. One design, the position-sensitive photomultiplier tube (PS-PMT) (Kume *et al* 1986), provides two-dimensional position information via two sets of wire anodes that are arranged orthogonally to one another. The electrons from the last dynode stage are read out on each set of anode wires. The position of the incident light on the photocathode can be estimated from the electron distribution on each set of anodes. Readout of the wire anodes is typically accomplished via separate internal resistive chains for x- and y-dimensions, resulting in a total of four channels that must be digitized and processed (Kume *et al* 1986). While PS-PMTs of this type can offer a large area (up to 5 inch diameter), they are also characterized by relatively large dead regions on the periphery that limit the ability to effectively assemble arrays of tubes to enlarge the detector area. Consequently, they have primarily been used in single-tube camera assemblies for small field-of-view applications (Del Guerra *et al* 2006).

The latest generation of position-sensitive PMTs utilizes metal channel dynodes for charge multiplication with individual anode outputs (Kyushima *et al* 2000). Sometimes referred to as multi-anode PMTs (MA-PMTs), these tubes have a compact, flat-panel design with smaller dead regions at the edges than earlier PS-PMTs, making them better suited for tiling together to cover a large detector area. Examples of MA-PMTs of this type include the Hamamatsu H8500, the Burle 85011-501 Planacon and the Photonis XP9120-64. The Hamamatsu H8500, probably the best-known MA-PMT, offers an 8×8 array of anode outputs and has an external size of 52 mm $\times$ 52 mm $\times$ 15 mm. It has a square profile with a dead zone around the periphery of 1.5 mm, resulting in 89% effective area coverage. Rather than read out each anode output individually, some investigators have employed charge-division readouts that effectively reduce the 2D position information into a set of X and Y projection signals (Popov *et al* 2003). This reduction of $M \times N$ anode outputs into $M + N$ signals for digitization can be extended to multiple MA-PMT array assemblies by appropriate daisy-chaining of the signal lines, although doing so can negatively impact the count-rate capability of the detector. As with conventional Anger Cameras, estimating positions from linear combinations of signals leads to pincushion-like distortions that must be corrected in the case of a continuous crystal. For crystal arrays the decoding of the crystal in which an interaction occurred is generally accomplished through the use of a lookup table generated from a flood image, with the distortions often making it difficult to unambiguously identify crystals in the corners or along edges, as can be seen in figure 5.

The photodiode is an alternative method of converting scintillation light into an electrical signal. Choong and colleagues designed a compact camera made up of detector modules consisting of 8×8 photodiode arrays with each photodiode coupled 1-to-1 with a CsI(Tl) crystal (Choong *et al* 2002). The small size of these solid-state devices is appealing; however, the lack of signal amplification in standard photodiodes and the significant capacitance of the electrodes limit the signal-to-noise ratio. A higher performance relative of the photodiode is the silicon drift detector (SDD), shown in figure 7, a specialized design where electrons drift

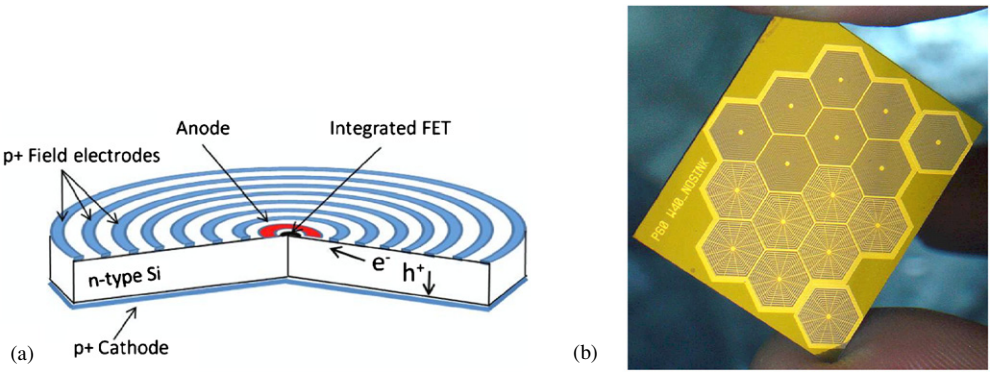

Figure 7. (a) Schematic drawing of a SDD. The electron collecting side is patterned with a set of concentric electrodes that create a horizontal drift field that guides the electron charge cloud to a very small collection anode. (b) Array of hexagonal SDDs (courtesy of Brookhaven National Laboratory).

toward a very small anode with low capacitance (Gatti and Rehak 1984, Fiorini *et al* 2000). SDDs offer high quantum efficiency for the detection of scintillation light, while their low capacitance and integration of front-end JFETs into the SDD chip provide low-noise operation, resulting in outstanding energy resolution. Up to 77 hexagonal SDDs have been fabricated in a close-packed, monolithic array covering 6.7 cm^2 for creation of a compact CsI camera (Fiorini *et al* 2009b). Alternatively, individual SDDs with larger active areas can be tiled to cover a greater total area (Fiorini *et al* 2008, Carini *et al* 2009).

Another attractive alternative to the photodiode is to utilize avalanche photodiodes (APDs). Like conventional photodiodes, APDs are compact, but they operate at higher reverse-bias voltages in a breakdown mode in which signal amplification occurs due to the acceleration of the drifting charges to the point where they themselves create additional electron–hole pairs. Imaging detector configurations can be created with either tiled APD arrays (Shah *et al* 2001) beneath a continuous crystal, in a manner similar to the standard Anger Camera, or else by using segmented scintillator crystals with a one-to-one coupling of crystal and APD. It remains challenging to achieve gain uniformity across the APD active area and maintain stability over time and temperature variations.

Position-sensitive avalanche photodiodes (PSAPDs) represent a special class of APDs in which spatial information about the photon distribution reaching the APD is made available via the application of a resistive layer on one face that also contains multiple contacts (Shah *et al* 2002). The resistive layer results in charge being shared among the contacts. The size of the signal reaching each of the four corners depends on the interaction position, while the sum of these signals provides an estimate of the total energy. For a configuration like that depicted in figure 8, initial estimates of the X and Y interaction positions are calculated according to $X = \frac{(S_3+S_2)-(S_4+S_1)}{S_1+S_2+S_3+S_4}$ and $Y = \frac{(S_4+S_3)-(S_1+S_2)}{S_1+S_2+S_3+S_4}$. These simple calculations typically exhibit the pin-cushion spatial distortions characteristic of Anger arithmetic in flood images, and some secondary position estimation correction, generally involving either a look-up table or a model of the spatial response (Despres *et al* 2007), is used to improve the spatial accuracy. An alternative signal combination method has been suggested by Zhang *et al* that reduces the spatial distortions to some degree (Zhang *et al* 2007). With any of these approaches, correctly resolving positions near the edges and corners is problematic and effectively reduces the useful field of view of individual devices with implications for cameras composed of tiled PSAPDs. In contrast to PMTs, APDs generally require cooling to reduce the leakage current to a level

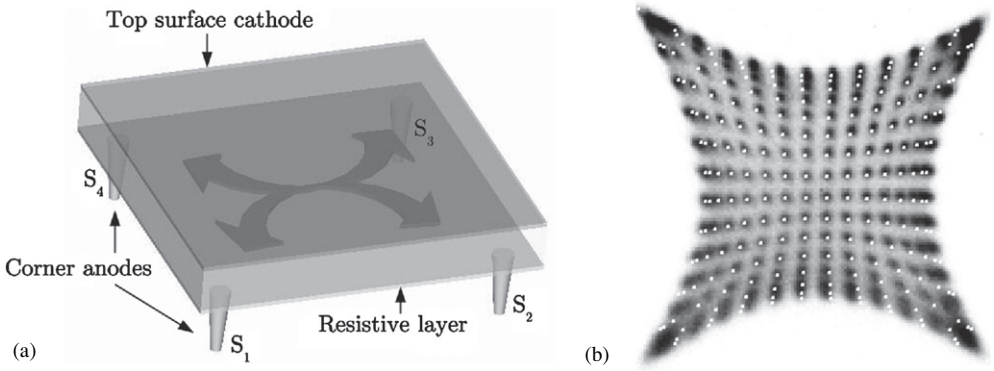

Figure 8. (a) Schematic representation of a PSAPD showing the four contacts at the corners of the resistive layer with arrows indicating the charge division in the resistive layer. (b) Raw flood image from PSAPD readout of a scintillator-crystal array. The superposed white dots are from a simulation of the charge-division process. From Despres *et al* (2007), © 2007 IEEE.

that does not adversely affect the energy resolution. Temperature stability is required as well because APDs exhibit temperature-dependent gain.

Charge-coupled devices (CCDs) and CMOS detectors have also found use as transducers for scintillator-based imaging detectors. While the readout of both PMTs and APDs is event driven, CCDs are read out in a frame transfer mode in which each pixel is read out in sequence after some integration period. Unambiguous identification of individual photon interactions under reasonable count-rate scenarios requires not only short integration times but rapid readout to minimize detector dead time. CCDs have high quantum efficiency, but the achievable energy resolution is influenced by dark current and readout electronic noise, the latter of which increases with increasing clock rate (Robbins and Hadwen 2003). In addition to cooling CCDs to reduce dark current, some CCD-based gamma-ray detector systems utilize electron-multiplying CCDs (EMCCDs) (Madan *et al* 1983, Jerram *et al* 2001) that employ a series of multiplying registers to amplify the charge signal during readout to minimize the impact of the readout noise on energy resolution. Since the active areas of CCDs are typically small in comparison to the desired size of a scintillator detector (CCD pixels are often $\sim$20 μm on a side), some form of de-magnification typically is employed in the coupling of the scintillator to the CCD to extend the detection area while retaining high intrinsic spatial resolution. Fiber optic tapers (de Vree *et al* 2005) and lenses (Nagarkar *et al* 2006, Soesbe *et al* 2010) have both been used to accomplish this coupling with minification between scintillator and CCD (figure 9(a)). Lens and fiber optic coupling always involves light loss, which carries implications for energy and spatial resolution for such approaches. Demagnifier (DM) tubes (Meng 2006) have been used to provide optical gain that partially compensates for the light loss that accompanies minification (figure 9(b)). Generation 2 image intensifiers with microchannel plates (Miller *et al* 2008) also have been used to elevate the signal from single scintillation photons well above the readout noise of commodity CCD and CMOS cameras, which both offer the advantages of room-temperature operation and fast frame rates (figure 9(c)).

An individual x ray or gamma ray interacting within the scintillator gives rise to many optical photons emitted isotropically, resulting in signals in multiple pixels. Despite this signal spread, CCD- and CMOS-based detector systems can offer excellent intrinsic spatial resolution ($\sim$250 μm) even in integrating mode where the projection image is formed by simply

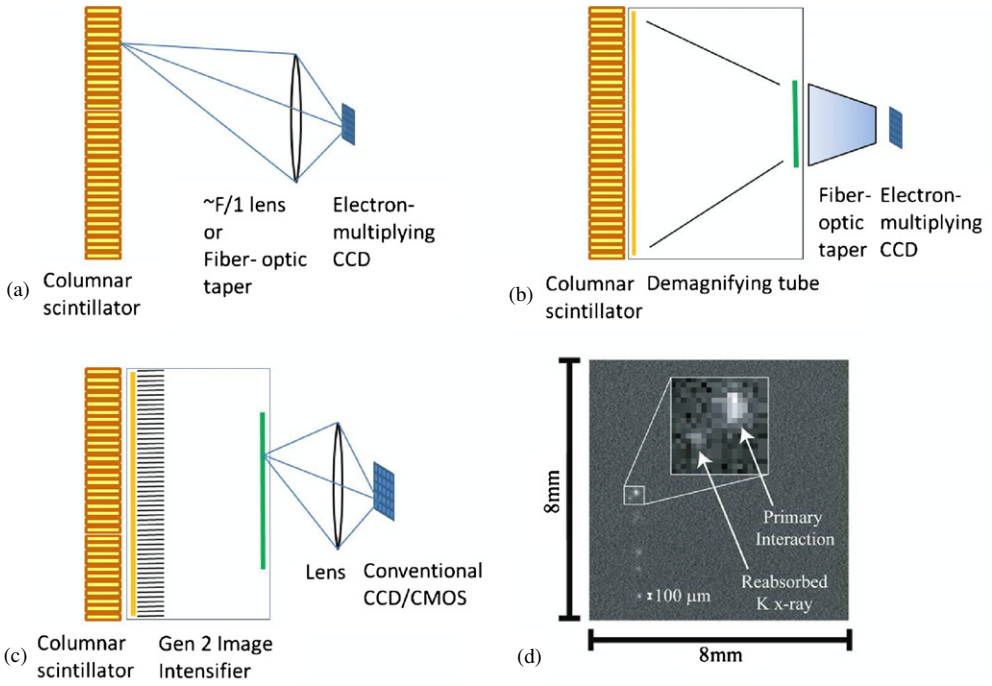

Figure 9. Principal CCD/CMOS SPECT camera geometries employing columnar scintillators and capable of photon counting: (a) direct lens-coupled (or fiber-optics-taper-coupled) EMCCD system; (b) demagnifying tube and fiber-optic-coupled EMCCD; and (c) image-intensified and lens-coupled conventional CCD or CMOS camera. (d) Single frame from an EMCCD showing a primary gamma-ray interaction along with a reabsorbed secondary x ray (courtesy of B W Miller, University of Arizona).

summing the signals from individual frames (Beekman and de Vree 2005). However, the intrinsic resolution can be improved significantly when operating in a photon-counting mode in which each frame is processed to identify signal clusters arising from individual gamma-ray/x-ray interactions and to estimate the centroids of these clusters. This approach has been demonstrated to yield intrinsic spatial resolutions down to ~50 μm FWHM (Beekman and de Vree 2005, Heemskerk *et al* 2007, Miller *et al* 2008). In photon-counting mode, the energy of each incident photon also can be estimated although the energy resolution estimated by simply summing the signal across all pixels in a cluster is generally poor in comparison to traditional PMT-based detector systems. One of the complicating factors in both energy and position estimation of individual events is that, even if the incident photon underwent photoelectric absorption, multiple clusters can be created due to the propagation and subsequent interaction of the K x ray resulting from the filling of the electron vacancy created in the initial interaction. Remarkably, the reabsorption of the secondary x ray can often be seen as a distinct companion event due to the outstanding spatial resolution, as shown in figure 9(d).

The large pixel counts and high frame rates of CCD- and CMOS-based systems generate enormous amounts of data, even though only a small number of pixels within any frame contain relevant information about photon interactions. The advent of general-purpose computing on graphics processor units (GPCGPU) has brought sufficient processing power to allow real-time processing of frame data to create list-mode data consisting of either individual clusters or fully estimated position and energy information (Miller *et al* 2008).

A relative newcomer to the arena of PMT alternatives that has generated considerable excitement is the silicon photomultiplier (SiPM) (Herbert *et al* 2006), sometimes also referred to as a solid-state photomultiplier (SSPM) or multipixel photon counter (MPC). SiPMs consist of an array of Geiger-mode avalanche photodiodes (GAPDs), each $\sim$20 μm on a side and having an integrated quenching resistor. Each detection element consists of a large number of GAPD microcells connected together in parallel. A current pulse is generated at the output whenever a photon is detected within an individual GAPD. The size of the output pulse depends on the number of microcells that fire, providing an output signal that is proportional to the number of incident photons, provided each microcell on average sees less than one photon. These devices combine the compactness and low bias voltages of APDs with the high gain ($>10^6$) and stability of PMTs, but unlike these technologies, there are potential saturation issues from the all-or-none firing of individual microcells and their recovery time. By vetoing any outputs when only single microcells are above threshold, background from thermal excitation is effectively suppressed. The area of the detector is divided between the photodiode area and supporting unit-cell circuitry, which reduces the quantum efficiency. Modern CMOS camera sensors have finessed this issue by incorporating lenslet arrays that focus light that hits the unit cell onto the photosensitive area, but at present SiPMs are characterized by low fill factors that leave some questions as to their eventual importance for SPECT applications. Modeling of SiPM response and investigations of their statistical properties have begun (van Dam *et al* 2010), and further work is needed to understand the energy and spatial resolutions achievable in an imaging detector.

There also may be advantages in combining multiple readout methods to a scintillator camera. Heemskerk *et al* reported on a system in which an EMCCD was coupled to the back surface of a monolithic scintillator crystal with SiPMs mounted on the sides (Heemskerk *et al* 2010). The SiPMs detect light from scintillation events that otherwise would have been lost on the sides, and this information can then be used as *a priori* knowledge of the number of events contained within a given frame of EMCCD data. The addition of this data improves the rejection of noise events, reducing background.

Advances in semiconductor detectors

Semiconductor radiation detectors represent the main alternative to scintillator-based single-photon imaging systems. Being so-called direct-conversion devices, a major appeal of semiconductor detectors in comparison to scintillators is that they avoid the random effects associated with scintillation light production, propagation and conversion to an electrical signal. When a gamma ray interacts in a semiconductor detector, whether through a photoelectric interaction or Compton scattering, one or more energetic electrons are created. Each electron loses energy as it propagates via two primary competing processes: ionization and phonon generation. The ionization creates electron–hole (e–h) pairs, where a hole is the positively-charged electron vacancy in the valence band left when the electron has been promoted into the conduction band. Application of a bias voltage creates an electric field that causes the two types of charge carriers to drift in opposite directions. These moving charges induce transient current signals on the detector electrodes that can be sensed by an external electric circuit, thereby providing the means to measure the detector's response to a gamma-ray interaction.

Semiconductor detectors offer several potential advantages over scintillators. Foremost among these is that the direct conversion of energy deposited by gamma-ray interactions into electron–hole pairs eliminates the optical-photon-to-electrical-signal transducer stage. In scintillators that step invariably involves loss of signal through incomplete photon collection

Table 2. Important properties of semiconductor materials used for SPECT detectors. Data are from Barber and Woolfenden (2006) unless otherwise noted.

	Density ($g\ cm^{-3}$)	Attenuation at 140 keV (cm^{-1})	Energy per e–h pair (eV)	Mobility-lifetime Electron ($cm^2\ V^{-1}$)	Mobility-lifetime Hole ($cm^2\ V^{-1}$)
Si	2.33	0.02	3.61	0.42	0.22
Ge	5.32	0.72	2.98	0.72	0.84
CdTe	5.85	3.22	4.43	3×10^{-3}	5×10^{-4}
CdZnTe	5.82	3.07	~5	3×10^{-3}	5×10^{-5}
HgI_2	6.40	8.03	4.20	$<10^{-2}$[a]	5×10^{-5}

[a] From Baciak *et al* (2002).

and the possibly low quantum efficiency of the converters. By avoiding the need for bulky PMTs, semiconductor imaging systems can also be made much more compact, reducing the amount of shielding and simplifying the mechanics in comparison to the Anger Camera. Additionally, the energy required to create an e–h pair in most semiconductors employed as radiation detectors is sufficiently small (see table 2); that is typical gamma-ray interactions generate a large number of charge carriers.

Moreover, the energy resolution of semiconductor detectors often exceeds what might be expected by applying a Poisson model to charge-carrier generation. The Fano factor is the ratio of the variance of a random variable to its mean (Fano 1947). Since the variance is equal to the mean for a system obeying Poisson statistics, such a system would have a Fano factor of 1 ($F = 1$). Typical values for semiconductor Fano factors are in the 0.05–0.2 range, meaning that in the absence of other noise sources energy resolution is several times better than would be predicted from applying Poisson statistics to the number of e–h pairs produced for a given energy deposition. The reason for this is that the efficiency of energy transfer to phonons, the primary process that competes with e–h production as an energy-loss mechanism of electrons, is low in semiconductors. Consequently, the production of e–h pairs is not a Poisson process because conservation of energy requires that the number of e–h pairs created be less subject to statistical fluctuations (Barrett and Myers 2004). In contrast, scintillators generally have Fano factors greater than 1 ($F > 1$) (Dorenbos *et al* 1995, Moses 2002), meaning an energy resolution worse than would be predicted from Poisson statistics, although there may be conditions under which certain high-light-output scintillators exhibit $F < 1$ (Bousselham *et al* 2010).

In practice the energy resolution of most semiconductor detectors is dominated by other noise sources (e.g. leakage current, electrode capacitance), and not the charge-carrier statistics, yet they generally do offer better energy resolution than scintillator-based systems (Radeka 1988). Table 2 lists the most common semiconductors used as imaging detectors and some of their relevant properties.

Another important aspect of semiconductor detectors is the ability to use photolithography to pattern electrode structures directly onto the detector surface. While some imaging systems have been fabricated from a collection of small, individual semiconductor detectors (Eisen *et al* 1996, Chambron *et al* 2000), most systems employ one or more detector crystals that themselves have multiple readout electrodes that offer more detailed spatial information on the location of the photon interaction within the crystal.

One method of obtaining spatial information from a semiconductor detector is to use so-called pixel detectors in which a series of square pixels are patterned on one detector side—typically the anode side. In this case, only a single side of the detector must be read out to

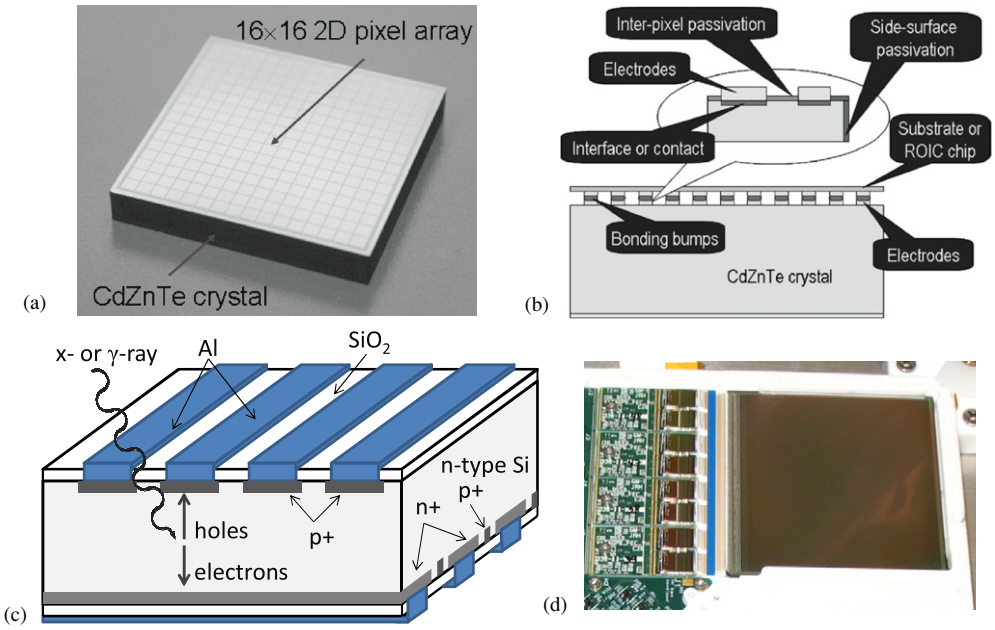

Figure 10. (a) Example of a 2D pixel detector. (b) In a pixel detector all electrodes can be bonded directly to the readout electronics. (c) Schematic view of a double-sided strip detector, which requires readout on two sides. (d) Photograph of a ∼36 cm^2 silicon DSSD with the ASICs and associated electronics for the 1024 strips on one side visible on the left. (a) and (b) Reprinted from Szeles *et al* (2008), © 2008 IEEE.

obtain two-dimensional position information. An alternative method is to fashion orthogonal strips on opposing sides of the crystal. In these double-sided strip detectors (DSSDs) charge signals must be read out from both sides in coincidence, and the two-dimensional interaction position of the incident photon must be estimated from the combination of strips with signal on each side. Figure 10 shows examples of both pixel detectors and DSSDs. The main advantage of the DSSD approach is that a smaller number of channels are needed: $2 \times N$ for an $N \times N$ detector, as opposed to N^2 channels for an equivalent pixel detector. However, the DSSD requires processing signals of both polarities, which involves the additional complication of decoupling the detector bias, while in a pixel detector all channels are of the same polarity and sit at the same potential. Large-area DSSDs can also suffer from degraded energy resolution due to the high capacitance associated with long strips, as well as ambiguity in event localization when there are multiple interactions in a short time interval. In either DSSDs or pixel detectors, the electrode structures can be fabricated with extremely fine feature sizes, down to ∼20 μm, although the intrinsic spatial resolution of a semiconductor device is not strictly given by the electrode pitch. On the one hand, charge diffusion effects can result in signals being generated across multiple channels, while on the other hand, with certain detector geometries it is possible to estimate interaction positions to sub-strip or sub-pixel levels using advanced signal-processing and position-estimation techniques (Marks *et al* 1999, Burks *et al* 2004).

Silicon is an appealing choice for an imaging detector owing to the availability of large, high quality crystals and the extensive experience in fabrication and instrumentation of both DSSD and pixel detectors for use in high-energy physics experiments. They also offer good energy resolution and can be operated at room temperature. The major drawback of silicon

is that its low atomic number results in modest detection efficiency at the photon energies of interest for most SPECT applications, but it is potentially applicable to imaging of x- and gamma-ray emissions from the decay of ^{125}I (27–35 keV), a radionuclide suitable for many small-animal imaging applications (Peterson *et al* 2003). While standard silicon detectors are 300 μm thick, the use of thicker detectors (1 mm) offers reasonable efficiency ($\sim$30%) for ^{125}I in combination with $\sim$60 μm spatial resolution (Shokouhi *et al* 2009). A unique property of these silicon DSSDs is the ability to stack detectors one behind the other, with the photons not detected in the first detector passing unimpeded to the second detector, increasing the overall detection efficiency while simultaneously collecting pinhole projection data at multiple magnifications. To further increase the detection efficiency (to $>$90%) for ^{125}I imaging, Choong and colleagues proposed a system based on 6 mm thick lithium-drifted silicon (Si(Li)) (Choong *et al* 2005). Besides low-energy small-animal imaging, the other area of nuclear medicine where silicon detectors have been utilized is as the scatter detector in a Compton camera (Meier *et al* 2002).

High-purity germanium (HPGe) is in some respects the ideal semiconductor detector material, as it offers outstanding energy resolution ($<$1% FWHM at 140 keV) and can also be processed into position-sensitive detector configurations (Luke *et al* 2000). The chief drawback of germanium detectors is that they have a relatively small bandgap, and consequently they must be operated at temperatures near 100 K to sufficiently suppress leakage currents for low-noise operation. The need for cumbersome cryogenics has precluded effective assembly into gamma cameras, particularly rotating gantry systems for SPECT. However, recent advancements in compact, Stirling-cycle mechanical cooling systems have eliminated the need for liquid nitrogen, making HPGe worthy of renewed consideration as a SPECT detector (Johnson *et al* 2011).

The most widely investigated semiconductors for nuclear medicine are CdTe and CdZnTe (CZT). Each offers a higher effective atomic number than silicon or germanium, and they can be operated at room temperature due to the 1.6 eV bandgap. To date, neither can be grown in as large-diameter single crystals as silicon or germanium, let alone NaI(Tl). Furthermore, crystal growth defects, such as twinning and polycrystalline domains, have deleterious effects on detector performance (Burger *et al* 2000), and often limit the size of the detectors that can be cut from the crystal boules or reduce the detector yield. CdTe also is subject to polarization (Bell *et al* 1974), which manifests itself as a loss of sensitivity and degradation of energy resolution over time while held at constant bias voltage. This phenomenon is thought to be related to ionization of deep acceptor levels but may also be influenced by surface states (Niraula *et al* 2002). Periodic switching of the bias can be employed to mitigate this effect (Siffert *et al* 1976, Ogawa *et al* 2009). CZT apparently is not immune to polarization effects, but they seem to appear only at high event rates such as encountered in transmission x-ray measurements (Szeles *et al* 2008).

Both CdTe and CZT generally suffer from reduced hole transport (relative to electron) in part due to hole trapping, which occurs at the site of crystalline defects such as vacancies or impurities. The impact of trapping on charge collection may be illustrated by considering one type of charge carrier (electron or hole) to have a single dominant trapping level with the traps uniformly distributed throughout the detector. Then the number of those charge carriers decreases exponentially with a mean lifetime τ. The charge carriers in semiconductors drift at constant velocity, $v = \mu E$, where μ is the mobility of that charge carrier in the material and E is the electric field created by the applied bias voltage. If a gamma-ray interaction creates

N_0 e–h pairs at a depth x in a planar detector of thickness L, then the induced charge on the electrode is given by the *Hecht* relation (Akutagawa and Zanio 1969):

$$Q = qN_0\left[\frac{\mu_h\tau_h E}{L}(1 - e^{-x/\mu_h\tau_h E}) + \frac{\mu_e\tau_e E}{L}(1 - e^{(x-L)/\mu_e\tau_e E})\right]. \quad (2)$$

As can be seen from equation (2), in a planar electrode configuration the product of the mobility and lifetime, two intrinsic properties of the crystal, governs the contribution of each charge-carrier type to the measured signal. While increasing the electric field via the application of a higher bias voltage improves the charge collection, the accompanying increase in leakage current increases noise (Luke *et al* 2001), creating a trade-off. The relatively poor hole mobility-lifetime ($\mu\tau$) product in CdTe and CZT (see table 2) gives rise to a depth dependence in signal generation that manifests itself as a low-energy tail on the photopeak of the pulse-height spectrum. While the photopeak itself may be quite narrow, inviting the application of a narrow energy window to suppress Compton-scattered photons, such energy windowing can severely compromise the detection efficiency as upward of 60% of events may be subject to tailing effects (Hruska and O'Connor 2008). Several electrode configurations have been developed that reduce sensitivity to hole trapping through single-polarity charge sensing.

By dividing the positive electrode into pixels whose linear dimensions are several times smaller than the detector thickness, the signal sensed on a pixel will be due almost entirely to electrons. This is the so-called small-pixel effect (Barrett *et al* 1995b). Decreasing the pixel size both reduces the influence of holes on the signal and improves the spatial resolution, but at some point these improvements are offset by the distribution of charge across multiple pixels, resulting in the need to read out pixel neighborhoods (Kim *et al* 2006). The balance between these effects is determined by the distance scale over which charge is created (fluorescence x rays) and diffusion of the electron cloud, so the optimal pixel size depends on the detector material and thickness.

Another approach is the orthogonal-coplanar-anode strip detector, a variation on the coplanar-grid detector design (Luke and Eissler 1996) that features row by column readout on a single detector side (Macri *et al* 2004). Each row is a series of interconnected pixel electrodes, while each column is a continuous-strip electrode with cut-outs that encircle the pixels. By biasing the strip electrodes at a potential between those of the pixels and the cathode on the opposing surface, electrons are collected on pixels, providing energy and position information on one dimension, while the strips provide position information in a second dimension through signals induced by the motion of the electrons to the pixels.

Alternatively, hole trapping can be used to advantage by reading out signals on both sides of the detector, employing single-polarity charge sensing on the anode side and then using the ratio of the trapping-degraded signal on the cathode to the anode signal as a means of estimating the depth of interaction (He *et al* 1999).

Mercuric iodide (HgI_2) is another compound semiconductor that has attracted interest for nuclear medicine applications for some time (Levi *et al* 1982, Patt *et al* 1989, Schieber *et al* 1983). HgI_2 is appealing in that it not only offers high density, leading to good stopping power, but also has a high effective atomic number, resulting in a higher photoelectric absorption probability at 140 keV than CdTe or CZT. The major drawbacks to HgI_2 are that the crystals are soft, making it a difficult material with which to work, and that they can be stoichiometrically unstable. HgI_2 also exhibits poor mobility for both holes and electrons, and thus must be operated at high bias voltages to achieve sufficient charge carrier collection for good energy resolution. Two other room-temperature, compound semiconductors that have some potential as imaging detectors are PbI_2 and TlBr. Like HgI_2, both of these semiconductors have very good stopping power, but to date neither has reached the level at which commercial-scale

fabrication is possible. A particularly intriguing possibility for all of these materials is to manufacture complete detector modules via deposition procedures directly onto the readout (Zentai *et al* 2005, Hartsough *et al* 2009).

Advances in semiconductor readout

The high degree of granularity afforded by either DSSDs or pixellated semiconductor detectors necessitates a large number of electronics channels if each detector element is to be read out individually. Even fairly modest systems can require thousands of channels, making discrete electronics impractical. Consequently, most semiconductor systems employ some form of application-specific integrated circuit (ASIC) for the electronics readout. It is worth noting that the increasing use of semiconductor-based photodetectors (PSAPDs, SDDs, SiPMs) for scintillators likewise results in the need to deal with large numbers of semiconductor signals, leading to the adoption of ASIC-based readout for many scintillator cameras (Gola *et al* 2008). There are three basic approaches in ASIC architecture: the gated integrator, self-triggering and binary counter.

The clocked gated-integrator approach (Marks *et al* 1996) shares similarities with CCD and CMOS readout in that a fixed acquisition period is followed by readout of the accumulated signals on all channels. One benefit of gated integrators is that the control logic and readout is straightforward. Reading out every channel of every frame generates an enormous amount of data that must be sifted through to identify events, and, because leakage current is also integrated, event identification requires application of a threshold after baseline subtraction. Gated integrators also are subject to so-called kTC noise arising from the switching of the reset circuit, although this can be addressed by using a correlated-double-sample-and-hold technique (Hynecek 1992, Augustine 1994). The use of buffering minimizes the dead time associated with readout, and analyses have shown that multiple events can be identified within a frame, so event rates of at least 10 kcps can easily be sustained in megapixel devices acquiring frames at 100 Hz as long as conditions limiting spatial overlap are met (Furenlid *et al* 2000).

In a self-triggering, event-driven ASIC such as the one described in Pettersen *et al* (2005), each electronics channel includes a discriminator that generates a logic pulse initiating the readout cycle whenever a signal exceeds a threshold. Leading-edge discriminators are the most common choice because they require less power than constant-fraction discriminators, and often trim DACs are included for each channel to allow for compensation of threshold variations arising from gain and offset differences among channels. Generally, such ASICs include separate fast-shaping and slow-shaping amplifiers, with the fast-shaper signal going to the discriminator and the slow-shaper signal output going to a sample-and-hold or peak-hold circuit. When an event trigger is generated, control logic then either clocks out every channel, only the channel that generated the trigger, or the trigger channel and a select group of neighboring channels—the latter processes referred to as sparse readout. While selection and readout of the neighbors is straightforward in the case of a strip detector, the process is more complicated in a pixel detector as the channels of interest are not consecutive. Noisy channels in self-triggering systems can create dead-time losses and large list-mode files, so most ASICs have a provision for turning off individual channels.

A third approach to ASIC architecture, exemplified by the Medipix2 chip (Llopart *et al* 2002), is to equip each channel with one or more binary counters tied to the discriminator outputs. After a specified counting interval, the number of events recorded in each channel is then read out. This approach offers a high count-rate capability and is employed, for example, in some photon-counting x-ray detector systems (Pangaud *et al* 2007, Butler *et al* 2008, Schlomka *et al* 2008), but it does not allow for in-depth analysis of individual events,

(a) 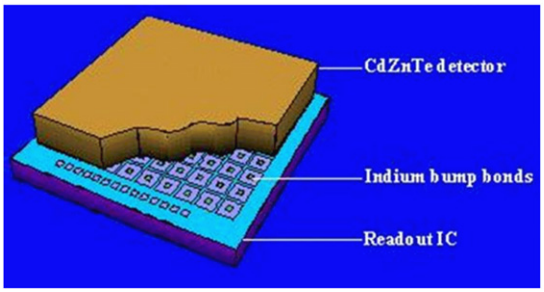

(b) 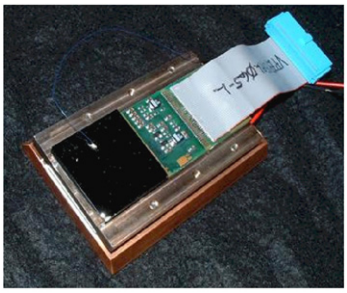

Figure 11. Schematic (a) and photo (b) of a CZT pixel detector bump-bonded directly to an *Arizona* readout ASIC. Also visible in (b) is a matching thermoelectric cooler and copper heat exchanger.

precluding any advanced position estimation based on charge sharing across electrodes. The Medipix3 chip (Ballabriga *et al* 2007), however, does include pixel-summing circuitry to properly capture events that might otherwise not pass threshold due to charge spreading across neighboring pixels.

In DSSDs, the ASICs are located on the edges and connected to the individual strips via wirebonds. This layout limits the ability to tile multiple detectors into a larger active area beyond a 2×2 configuration. In principle, multiple detectors could be chained together and connected to a common readout, as is done in some barrel detectors for collider experiments (Hazumi 1996, Gaidarev 1996), but assembly of such systems is complicated and the joining together of strips from multiple detectors can lead to large electrode capacitances that degrade performance.

In principle the single-sided readout of pixel detectors provides better opportunity than DSSDs to tile multiple detectors into a large-area camera. However, the process of connecting individual pixels to the electronics readout can be challenging. While some investigators have directly bonded the pixels to the readout ASIC, for example the 64×64 pixels CZT detectors (shown in figure 11) developed at the University of Arizona in which both detector and readout measure $1'' \times 1''$ (Matherson *et al* 1998), there is generally a mismatch in size between the detector and ASIC, so an interposer is commonly used between the detector and the ASIC to route the pixel signals to the individual preamp inputs.

Commercial CdTe and CZT hybrids like those shown in figure 12, comprising slabs of pixellated detector bonded to matching readout circuits, have been produced in a variety of configurations, with pixel pitches ranging from approximately 2.0 to 2.5 mm, by several companies including Ajat, EI Detection & Imaging Systems (formerly eV Products), Gamma Medica-Ideas and Orbotech. Clinical gamma cameras have been developed by tiling together dozens of these modular CdTe and CZT detectors to cover areas similar to conventional Anger Cameras (Eisen *et al* 2002, Wagenaar *et al* 2003, Petrillo *et al* 2004). Smaller assemblies of modular CZT pixel detectors have been deployed for scintimammography (Mueller *et al* 2003, O'Connor *et al* 2006), where the higher energy resolution allows for narrower energy windows, reducing scatter from the torso. These same modules and cameras also find application in cardiac and small-animal SPECT systems (Parnham *et al* 2006, Volokh *et al* 2008, Gambhir *et al* 2009). All of these devices have pixel dimensions comparable to the intrinsic resolutions in scintillation cameras.

The direct bonding of semiconductor detector materials other than Si to readout ASICs presents the problem of differential thermal expansion and the challenge of how to keep the

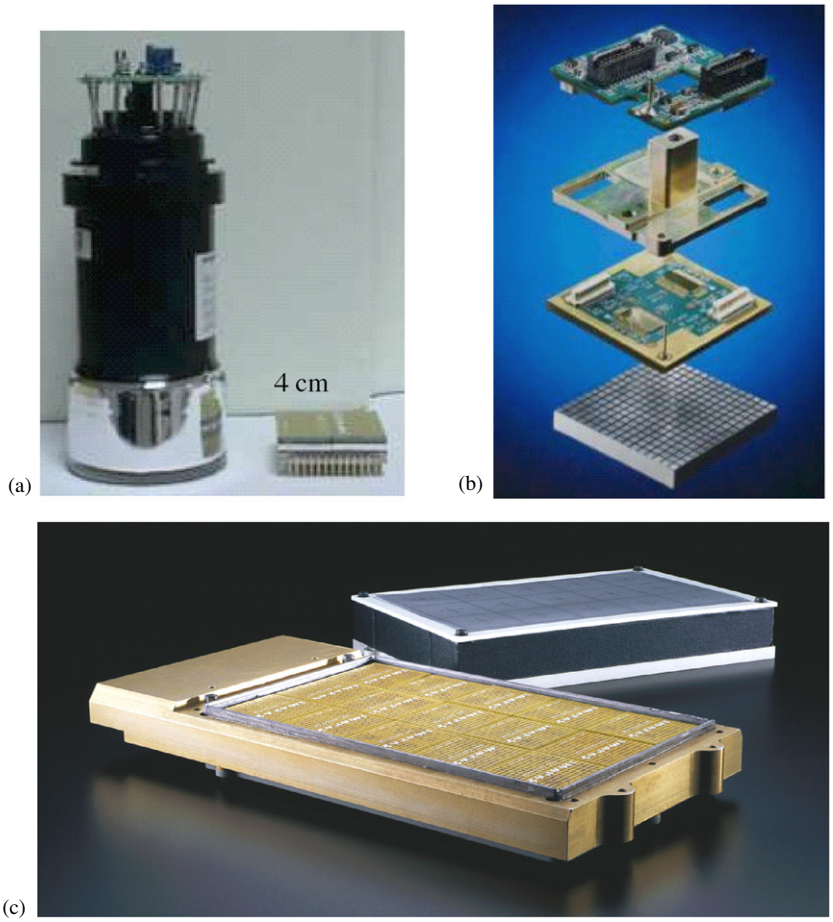

Figure 12. (a) Photo of a CZT hybrid beside a PMT illustrating the compact nature of a semiconductor-based system. (b) Exploded view of the components of a CZT hybrid including detector crystal, readout ASICs and interconnects. (c) Prototype gamma camera made up of 15 CZT hybrids similar to those shown in (a) and (b) is shown alongside its outer casing. (Images in (a) and (b) courtesy of A Peretz, GE Healthcare, (c) courtesy of Siemens Healthcare.)

detector/readout assembly from separating during repeated thermal cycling. The use of soft bonds, such as indium bump bonds, has been fairly successful, though an underfill of epoxy seems necessary to prevent eventual delamination. The long-term stability of CZT detectors with temperature and humidity variations has been studied, and not found to be a problem under moderate conditions (Maehlum *et al* 2007).

Advances in signal processing and estimation

The formation of a projection image by photon-counting detection of emitted x rays and gamma rays always involves inversion of raw signals to extract event parameters. Even in the extreme case of a camera composed of an array of discrete detectors, a decision of whether an individual event should be included in the image requires the estimation of the energy of the incident photon.

In general, the event properties to be estimated from the signals read out from a SPECT detector are the two-dimensional coordinates of the interaction position and the energy deposition. This is especially true with parallel-hole collimators, which select for gamma rays entering the detectors at close to normal incidence. Sometimes the influence of scattering within the subject is ignored, in which case no energy estimate need be made. On the other hand, most small-animal SPECT systems now employ pinhole collimation that accepts oblique incidence angles such that an unresolved depth of interaction of the incident photon contributes to a parallax blur. The effort to maximize final reconstructed-object resolution may then involve estimation of energy deposition and interaction position in all three dimensions.

It is possible to employ signal-processing methods of different levels of mathematical rigor to these estimation tasks. The traditional algorithms were chosen based on ease of implementation and execution speed in the era preceding fast desktop computers. These estimation procedures often involve multiple steps, such as application of Anger arithmetic to a collection of PMT signals followed by a heuristic correction to the event positioning to compensate for the inherent distortions in the initial calculation. Similarly, data from pixellated scintillators can be converted to a position estimate using Anger arithmetic and from the resulting x–y coordinates an assignment can then be made as to which crystal the photon interacted in, often employing a lookup table. This process requires prior acquisition of a flood map from which crystal boundaries are delineated, allocating a range of x–y Anger-derived values to a particular crystal and substituting its centroid as the interaction position.

In the new scintillation camera designs that use CCD or CMOS detectors, as shown earlier in figure 9, substantial in-line signal processing is required in order to identify and isolate events from the large amount of pixel data generated in each frame. In these devices, frame rates ($\sim$25–200 frames per second are typical) are fast enough that individual gamma rays may be counted, but their locations in the frames must be found and the pixel neighborhoods with scintillation light extracted in the short time between frames. The alternative of saving unprocessed frames quickly exhausts storage media. The algorithms may involve dark-current subtraction, median filtering, thresholding, cross-correlation scanning of the 2D raster with a template to locate event centers, and a means for determining how large a region of the image to associate with each center (Miller *et al* 2008, 2009a, Korevaar *et al* 2009b). In the past, this kind of digital processing was the domain of dedicated digital signal processors (DSPs), but in the new systems GPUs tend to be employed, with recent hardware providing enough computing power to handle several megapixel cameras at once, each running at $>$100 frames per second. Of course, once pixel clusters have been extracted, these devices too require the application of estimation methods to yield information about the gamma-ray interaction.

Regardless of the detector technology, the random nature of the signal-generation process and electronic noise create an uncertainty in the relation between the signals and the event properties that can be accounted for if statistical estimation methods are used to process the experimental data. Statistical estimation techniques also offer the appealing advantage of providing an additional criterion to filter on, namely the likelihood (Barrett and Myers 2004, Barrett *et al* 2009), that can improve the imaging performance of the detector. Likelihood thresholding (Milster *et al* 1990) can, for example, eliminate events that create data inconsistent with the forward model, such as if energy from a single gamma ray is deposited in multiple areas in the detector due to a Compton interaction followed by a long propagation of the scattered photon. In this case, the pattern of detector signals has a low probability of resulting from a single, local interaction, allowing the event to be rejected rather than contribute blur to the image.

The application of ML methods to signal processing for SPECT detectors offers particular advantages (Barrett *et al* 2009), including being asymptotically unbiased, i.e. requiring no

distortion corrections in the limit of large numbers of counts, and being fast to compute using parallel architectures such as GPUs (Hesterman *et al* 2010). ML-estimation also has been used to extract depth-of-interaction information from Anger Camera-like geometries (Gagnon *et al* 1993, Hunter *et al* 2009). The application of ML methods can generally be formulated in terms of a search over all possible event attributes, $\boldsymbol{\theta}$, to find the estimate, $\hat{\boldsymbol{\theta}}$, that has the highest probability of generating the observed measurements $\mathbf{g}$:

$$\hat{\boldsymbol{\theta}} = \arg\max_{\theta}(\text{prob}\,(\mathbf{g}\,|\theta\,)). \tag{3}$$

Evaluating the probability for a given $\boldsymbol{\theta}$ requires knowledge of the forward model and its statistical properties. These can generally be found through a combination of physical modeling and calibration measurements. A common way of calibrating gamma cameras for use with ML estimation is with collimated pencil beams that are scanned across the camera face in a regular pattern (Chen *et al* 2005). By directly measuring the position dependence of the signals, minor imperfections in the scintillator crystal or optical coupling can be compensated for, but the procedure requires access to the camera and a suitable stage system for translating the source. The benefits of careful pencil-beam calibration and statistical estimation are by no means restricted to scintillation detectors. For example, Marks *et al* used this method to correct for local flaws in a CZT pixel detector, and, as mentioned earlier, even demonstrate sub-pixel position estimation (Marks *et al* 1999).

Figure 13 summarizes the range of acquisition strategies that can be employed in going from raw detector signals to stored digital data (the fourth block depicted in figure 13). One trend in signal processing that is evident across detector types is packet-based information transmission between front-end electronics that extract event data and back-end data buffers that accumulate image data. The progress in fast serial-bus communications in commodity electronics has been a driving force, and developers of cameras have opted for USB (de Vree *et al* 2005, Schmid *et al* 2001), FireWire (Miller *et al* 2008), raw ethernet (Deprez *et al* 2011), TCP/IP and custom LVDS protocols (Furenlid *et al* 2004, Kim *et al* 2006). Another trend is to place sophisticated FPGAs in the front ends to process signal data in real time to extract event parameters as early as possible. As shown in figure 13, an alternative strategy is to retain all raw signals associated with each event in what might be termed 'super list-mode' acquisition. This strategy provides the greatest flexibility for post-processing after the completion of data acquisition. The rapid pace of developments in both embedded processors and desktop computer power makes this an evolving area.

Summary and future prospects

Despite the variety of approaches and the considerable progress made on many of the alternatives, presently the Anger Camera continues to be the dominant SPECT detector technology in the clinic. This is despite the fact that a variety of detector systems have demonstrated superior performance to the Anger Camera by one or more measures. An interesting way in which to compare competing detector technologies is in terms of their space-bandwidth products because it takes into account both the spatial resolution and the physical size of the detector. Table 3 provides representative space-bandwidth products of the basic unit elements for a number of different detector technologies. While the space-bandwidth product of the Anger Camera is respectable, essentially all of the other approaches would yield totals exceeding it if scaled to cover the same area via tiling together of multiple detector units. Meanwhile, the crossed-strip silicon (SiliSPECT) and CMOS/CCD-based scintillator (BazookaSPECT) detectors listed in table 3 provide extremely large space-bandwidth products in a relatively small footprint thanks to their sub-100 μm spatial resolution. In these two

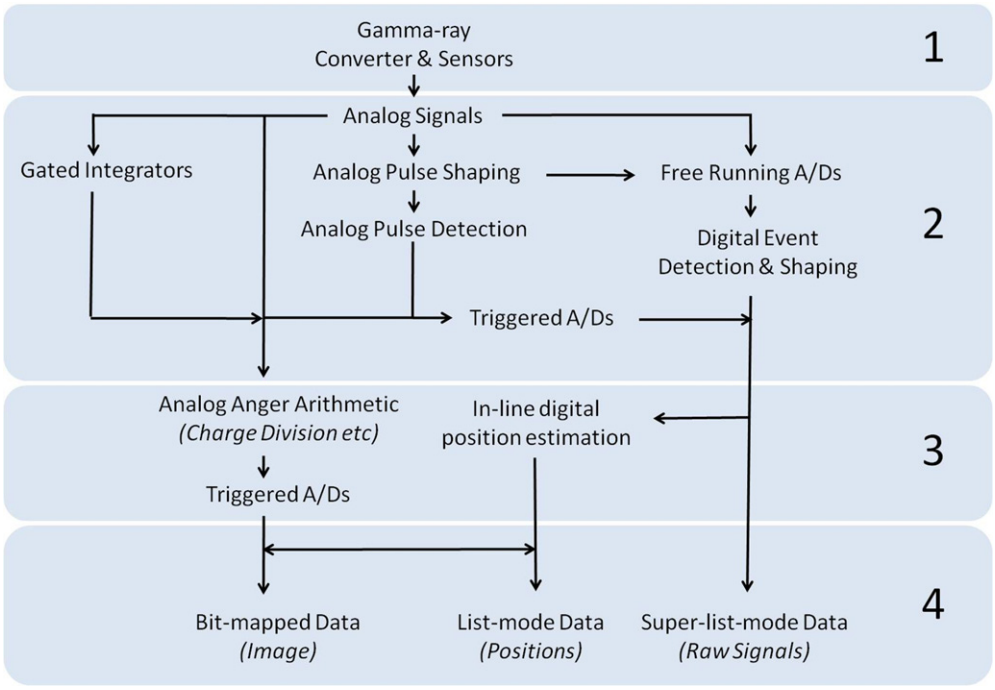

Figure 13. Graphical depiction of the variety of acquisition strategies that can be used with SPECT detectors to go from the chosen detector material (block 1) to stored data (block 4) with block 2 representing the readout and block 3 the estimation scheme.

Table 3. Space-bandwidth (SpBW) products and sizes of representative examples of several detector technologies.

Camera/ manufacturer	Material	Unit size	SpBW	Tileable	Reference
Anger Camera	NaI(Tl)	$\sim 50 \times 50 \times 1.0$ cm^3	$\sim 2 \times 10^4$	N/A	(Barrett and Hunter 2005)
MONICA	NaI(Tl)[a]	$4.2 \times 9.2 \times 1.0$ cm^3	798	Yes	(Xi *et al* 2010)
Orbotech	CdZnTe	$4.0 \times 4.0 \times 0.5$ cm^3	256	Yes	(Vadawale *et al* 2009)
Arizona Hybrid	CdZnTe	$2.5 \times 2.5 \times 0.2$ cm^3	4096	3 sides	(Barber *et al* 1997)
ERPC	CdTe	$1.1 \times 2.2 \times 0.1$ cm^3	2048	3 sides	(Meng *et al* 2009)
HICAM	CsI(Tl)	$1.2 \times 5.3 \times 1.0$ cm^3	$\sim$5000	3 sides	(Fiorini *et al* 2009a)
SiliSPECT	Si	$6.0 \times 6.0 \times 0.1$ cm^3	$>10^6$	2 sides	(Shokouhi *et al* 2009)
BazookaSPECT	CsI(Tl)[b]	5.0 cm Ø $\times$ 0.04 cm	$>2 \times 10^5$	Yes	(Miller *et al* 2009b)

[a] Pixellated.
[b] Micro-columnar.

particular cases, however, the detectors are optimized for low-energy ($\sim$30 keV) imaging, and it is unclear at present whether adaptation of these technologies to improve efficiencies at energies relevant for clinical imaging might impact their spatial resolution and, consequently, their space-bandwidth products.

An obvious factor in the persistence of the Anger Camera is its cost-effectiveness for covering large areas for human-body-imaging applications. Also contributing is the fact that

conventional parallel-hole collimation largely negates the spatial resolution advantages of competing technologies.

The same cannot be said for special-purpose applications, however, where competing approaches are being implemented in a variety of cardiac and breast scanners for two principal reasons: the ability to achieve improved energy resolution to reduce the effects of scatter and the ability to produce compact systems. Some of the cardiac SPECT systems employ many fixed or tilting cameras such that sufficient angular sampling is achieved without a rotating gantry, resulting in increased throughput capabilities. Improvements in detector spatial resolution, including depth-of-interaction capability, are also contributing to new thinking about collimator design for other applications with a goal of improving image resolution and/or sensitivity, and these developments may soon begin to loosen the grip of the Anger Camera on the nuclear medicine market.

In small-animal SPECT systems, where reconstructed resolutions are gradually approaching the 100 μm range, new technologies beyond the Anger Camera are almost certainly required since there is a need to achieve higher intrinsic spatial resolution while maintaining or improving sensitivity, eliminate parallax errors from depth-of-interaction effects and also create stationary imagers that facilitate dynamic SPECT measurements vital to understanding pharmacokinetics.

One arena in which the Anger Camera cannot compete is that of hybrid SPECT/MR systems because PMTs cannot function in strong magnetic fields. Most of the focus in the development of MR-compatible PET systems has been on the use of APDs or SiPMs as optical converters in scintillator-based systems. The additional need for a collimator for SPECT creates even greater space constraints inside of the magnet, making semiconductor-based systems the most attractive option for SPECT/MR. Systems utilizing CdTe (Jia-Wei *et al* 2009) and CZT (Hamamura *et al* 2010) currently are under investigation.

Technological developments that are likely to affect SPECT detector development include advances in light output from new scintillators, improvements in photomultiplier quantum efficiencies, faster frame rates in CMOS and CCD detectors, improvements in semiconductor crystal growth, and advances in readout ASICs and computing power. Recently, there has been considerable interest in applying vertical interconnects in silicon integrated circuits, which could in principle make it even more convenient to access all four sides of a detector plane for tiling. This new approach to 3D integration is accomplished with electrical connections via small holes through an ASIC that are filled with a conductive metal or epoxy, or via optoelectronic coupling (Bower *et al* 2006).

While PET often seems to receive more attention than SPECT, it is important to keep in mind that in clinical nuclear medicine SPECT usage far exceeds that of PET and that is likely to continue for some time. SPECT has a bright future both in clinical imaging and research due to its modest infrastructure requirements, correspondingly low costs, and the large number of approved and in-development radiotracers. The current demand for lowering radiation doses from medical procedures may provide additional impetus for innovation in clinical nuclear medicine that may eventually lead to the Anger Camera being displaced. Dose-lowering sensitivity increases coupled with improvements in energy resolution may also usher in more widespread use of dual-isotope imaging, which fits naturally with the hybrid imaging paradigm that has taken hold due to the benefits of multiple measures in assessing pathologies. The combination of the sizable clinical market and the unique challenges of preclinical imaging is likely to sustain interest in further developments of SPECT detector technologies in the years ahead.

Acknowledgments

The authors would like to acknowledge the contributions of H H Barrett, J M Woolfenden, H B Barber and B W Miller to many of the ideas and technologies presented here. This work was partly supported by the Office of Science (BER), US Department of Energy and by NIH grant P41 EB002035.

References

Akutagawa W and Zanio K 1969 Gamma response of semi-insulating material in the presence of trapping and detrapping *J. Appl. Phys.* **40** 3838–54

Anger H O 1952 Use of a gamma-ray pinhole camera for *in vivo* studies *Nature* **170** 200–1

Anger H O 1958 Scintillation camera *Rev. Sci. Instrum.* **29** 27–33

Augustine F L 1994 Multiplexed readout electronics for imaging spectroscopy of high-energy x-ray and gamma photons *Nucl. Instrum. Methods Phys. Res.* A **353** 201–4

Azevedo C D R, Silva A L M, Ferreira A L, da Luz H N, Moutinho L M, dos Santos J M F and Veloso J F C A 2011 2D-sensitive hpxe gas proportional scintillation counter concept for nuclear medical imaging purposes *J. Instrum.* **6** C01067

Baciak J E, He Z and DeVito R P 2002 Electron trapping variations in single-crystal pixelated HgI_2 gamma-ray spectrometers *IEEE Trans. Nucl. Sci.* **49** 1264-9

Ballabriga R, Campbell M, Heijne E H M, Llopart X and Tlustos L 2007 The Medipix3 prototype, a pixel readout chip working in single photon counting mode with improved spectrometric performance *IEEE Trans. Nucl. Sci.* **54** 1824–9

Barber H *et al* 1997 Development of a 64 × 64 CdZnTe array and associated readout integrated circuit for use in nuclear medicine *J. Electron. Mater.* **26** 765–72

Barber H B and Woolfenden J M 2006 *Nuclear Medicine* ed R E Henkin *et al* (St Louis, MO: Mosby) pp 137–53

Barrett H H, Denny J L, Wagner R F and Myers K J 1995a Objective assessment of image quality: II. Fisher information, Fourier crosstalk, and figures of merit for task performance *J. Opt. Soc. Am.* **12** 834–52

Barrett H H, Eskin J D and Barber H B 1995b Charge transport in arrays of semiconductor gamma-ray detectors *Phys. Rev. Lett.* **75** 156–9

Barrett H H and Hunter W C J 2005 *Small-Animal SPECT Imaging* ed M A Kupinski and H H Barrett (New York: Springer) pp 9–48

Barrett H H, Hunter W C J, Miller B W, Moore S K, Chen Y and Furenlid L R 2009 Maximum-likelihood methods for processing signals from gamma-ray detectors *IEEE Trans. Nucl. Sci.* **56** 725–35

Barrett H H and Myers K J 2004 *Foundations of Image Science* (New York: Wiley)

Beekman F J and de Vree G A 2005 Photon-counting versus an integrating CCD-based gamma camera: important consequences for spatial resolution *Phys. Med. Biol.* **50** N109–19

Bell R O, Entine G and Serreze H B 1974 Time-dependent polarization of CdTe gamma-ray detectors *Nucl. Instrum. Methods* **117** 267–71

Belyavskii Y D, Gulakov I R and Pertsev A N 1971 Scintillation (deexcitation) time of CsI(Tl) after gamma excitation *J. Appl. Spectrosc.* **15** 1331–4

Blazek K, De Notaristefani F, Maly P, Pani R, Pellegrini R, Pergola A, Scopinaro F and Soluri A 1995 YAP multi-crystal gamma camera prototype *IEEE Trans. Nucl. Sci.* **42** 1474–82

Blumgart H L and Yens O C 1927 Studies on the velocity of blood flow: I. The method utilized *J. Clin. Investig.* **4** 1–13

Bolozdynya A, Egorov V, Koutchenkov A, Safronov G, Smirnov G, Medved S and Morgunov V 1997 A high pressure xenon self-triggered scintillation drift chamber with 3D sensitivity in the range of 20–140 keV deposited energy *Nucl. Instrum. Methods Phys. Res.* A **385** 225–38

Bousselham A, Barrett H H, Bora V and Shah K 2010 Photoelectron anticorrelations and sub-Poisson statistics in scintillation detectors *Nucl. Instrum. Methods Phys. Res.* A **620** 359–62

Bower C A, Malta D, Temple D, Robinson J E, Coffinan P R, Skokan M R and Welch T B 2006 High density vertical interconnects for 3-D integration of silicon integrated circuits *56th Proc. Electronic Components and Technology Conf., 2006.* p 399–403

Bradley E L, Cella J, Majewski S, Popov V, Jianguo Q, Saha M S, Smith M F, Weisenberger A G and Welsh R E 2006 A compact gamma camera for biological imaging *IEEE Trans. Nucl. Sci.* **53** 59–65

Brem R F, Michener K H and Zawistowski G 2006 Approaches to improving breast cancer diagnosis using a high resolution, breast specific gamma camera *Phys. Med.* **21** (Suppl. 1) 17–9

Burger A, Chattopadhyay K, Chen H, Ma X, Ndap J O, Schieber M, Schlesinger T E, Yao H W, Erickson J and James R B 2000 Defects in CZT crystals and their relationship to gamma-ray detector performance *Nucl. Instrum. Methods Phys. Res.* A **448** 586–90

Burks M, Jordan E, Hull E, Mihailescu L and Vetter K 2004 Signal interpolation in germanium detectors for improved 3-D position resolution *Nuclear Science Symp. Conf. Record, 2004 IEEE* vol 2 pp 1114–8

Butler A P H, Anderson N G, Tipples R, Cook N, Watts R, Meyer J, Bell A J, Melzer T R and Butler P H 2008 Bio-medical x-ray imaging with spectroscopic pixel detectors *Nucl. Instrum. Methods Phys. Res.* A **591** 141–6

Carini G A, Wei C, De Geronimo G, Gaskin J A, Keister J W, Zheng L, Ramsey B D, Rehak P and Siddons D P 2009 Performance of a thin-window silicon drift detector x-ray fluorescence spectrometer *IEEE Trans. Nucl. Sci.* **56** 2843–9

Cassen B, Curtis L, Reed C and Libby R 1951 Instrumentation for 131I use in medical studies *Nucleonics* **9** 46–50

Chambron J *et al* 2000 A pixellated [gamma]-camera based on CdTe detectors clinical interests and performances *Nucl. Instrum. Methods Phys. Res.* A **448** 537–49

Chen Y C, Furenlid L R, Wilson D W and Barrett H H 2005 *Small-Animal SPECT Imaging* ed M A Kupinski and H H Barrett (New York: Springer) pp 195–201

Cherepy N J *et al* 2009 Scintillators with potential to supersede lanthanum bromide *IEEE Trans. Nucl. Sci.* **56** 873–80

Cherry S R, Yiping S, Siegel S, Silverman R W, Mumcuoglu E, Meadors K and Phelps M E 1996 Optical fiber readout of scintillator arrays using a multi-channel PMT: a high resolution PET detector for animal imaging *IEEE Trans. Nucl. Sci.* **43** 1932–7

Chiewitz O and Hevesy G 1935 Radioactive indicators in the study of phosphorous metabolism in rats *Nature* **136** 754–5

Choong W S *et al* 2002 A compact 16-module camera using 64-pixel CsI(Tl)/Si p-i-n photodiode imaging modules *IEEE Trans. Nucl. Sci.* **49** 2228–35

Choong W S, Moses W W, Tindall C S and Luke P N 2005 Design for a high-resolution small-animal SPECT system using pixellated Si(Li) detectors for *in vivo* ^{125}I imaging *IEEE Trans. Nucl. Sci.* **52** 174–80

de Vree G A, Westra A H, Moody I, van der Have F, Ligtvoet K M and Beekman F J 2005 Photon-counting gamma camera based on an electron-multiplying CCD *IEEE Trans. Nucl. Sci.* **52** 580–8

Del Guerra A *et al* 2006 Performance evaluation of the fully engineered YAP-(S)PET scanner for small animal imaging *IEEE Trans. Nucl. Sci.* **53** 1078–83

Deprez K, Van Holen R, Vandenberghe S and Staelens S 2011 Design of a high resolution scintillator based SPECT detector (SPECTatress) *Nucl. Instrum. Methods Phys. Res.* A **648** S107–10

Despres P, Barber W C, Funk T, McClish M, Shah K S and Hasegawa B 2007 Modeling and correction of spatial distortion in position-sensitive avalanche photodiodes *IEEE Trans. Nucl. Sci.* **54** 23–9

Despres P, Barber W C, Funk T, McClish M, Shah K S and Hasegawa B H 2006 Investigation of a continuous crystal PSAPD-based gamma camera *IEEE Trans. Nucl. Sci.* **53** 1643–9

Dorenbos P, de Haas J T M and van Eijk C W E 1995 Non-proportionality in the scintillation response and the energy resolution obtainable with scintillation crystals *IEEE Trans. Nucl. Sci.* **42** 2190–202

Eisen Y *et al* 2002 NUCAM3-a gamma camera based on segmented monolithic CdZnTe detectors *IEEE Trans. Nucl. Sci.* **49** 1728–32

Eisen Y, Shor A, Gilath C, Tsabarim M, Chouraqui P, Hellman C and Lubin E 1996 A gamma camera based on CdTe detectors *Nucl. Instrum. Methods Phys. Res.* A **380** 474–8

El Fakhri G, Moore S C, Maksud P, Aurengo A and Kijewski M F 2001 Absolute activity quantitation in simultaneous 123I/99mTc brain SPECT *J. Nucl. Med.* **42** 300–8

Fano U 1947 Ionization yield of radiations: II. The fluctuations of the number of ions *Phys. Rev.* **72** 26

Fiorini C *et al* 2009a First results of the HICAM anger camera *Nuclear Science Symp. Conf. Record, 2009 IEEE* pp 1891–3

Fiorini C, Gola A, Peloso R, Longoni A, Lechner P, Niculae A, Soltau H and Struder L 2008 Silicon drift detectors arrays for the HICAM gamma camera *Nuclear Science Symp. Conf. Record, 2008. IEEE* pp 2981–3

Fiorini C, Gola A, Peloso R, Longoni A, Lechner P, Soltau H and Struder L 2009b Imaging performances of the DRAGO gamma camera *Nucl. Instrum. Meth.* A **604** 101–3

Fiorini C, Longoni A and Perotti F 2000 New detectors for [gamma]-ray spectroscopy and imaging, based on scintillators coupled to silicon drift detectors *Nucl. Instrum. Methods Phys. Res.* A **454** 241–6

Franc B L, Acton P D, Mari C and Hasegawa B H 2008 Small-animal SPECT and SPECT/CT: important tools for preclinical investigation *J. Nucl. Med.* **49** 1651–63

Furenlid L R, Clarkson E, Marks D G and Barrett H H 2000 Spatial pileup considerations for pixellated gamma-ray detectors *IEEE Trans. Nucl. Sci.* **47** 1399–403

Furenlid L R, Wilson D W, Yi-chun C, Hyunki K, Pietraski P J, Crawford M J and Barrett H H 2004 FastSPECT II: a second-generation high-resolution dynamic SPECT imager *IEEE Trans. Nucl. Sci.* **51** 631–5

Gagnon D, Pouliot N, Laperriere L, Therrien M and Olivier P 1993 Maximum likelihood positioning in the scintillation camera using depth of interaction *IEEE Trans. Med. Imaging* **12** 101–7

Gaidarev P 1996 CLEO II silicon vertex detector *Nucl. Instrum. Methods Phys. Res.* A **379** 396–8

Gambhir S S, Berman D S, Ziffer J, Nagler M, Sandler M, Patton J, Hutton B, Sharir T, Haim S B and Haim S B 2009 A novel high-sensitivity rapid-acquisition single-photon cardiac imaging camera *J. Nucl. Med.* **50** 635–43

Garcia E V, Faber T L and Esteves F P 2011 Cardiac dedicated ultrafast SPECT cameras: new designs and clinical implications *J. Nucl. Med.* **52** 210–7

Gatti E and Rehak P 1984 Semiconductor drift chamber—an application of a novel charge transport scheme *Nucl. Instrum. Methods Phys. Res.* **225** 608–14

Genna S and Smith A P 1988 The development of aspect, an annular single-crystal brain camera for high-efficiency spect *IEEE Trans. Nucl. Sci.* **35** 654–8

Gola A, Bombelli L, Fiorini C, Frizzi T, Membretti G, Nava R and Peloso R 2008 A multi-channel ASIC for the readout of the HICAM gamma camera *Nuclear Science Symp. Conf. Record, 2008. IEEE* pp 1810–4

Goorden M C, Rentmeester M C and Beekman F J 2009 Theoretical analysis of full-ring multi-pinhole brain SPECT *Phys. Med. Biol.* **54** 6593–610

Gruber G J, Moses W W, Derenzo S E, Wang N W, Beuville E and Ho H 1998 A discrete scintillation camera module using silicon photodiode readout of CsI(TI) crystals for breast cancer imaging *IEEE Trans. Nucl. Sci.* **45** 1063–8

Hamamura M J, Ha S, Roeck W W, Muftuler L T, Wagenaar D J, Meier D, Patt B E and Nalcioglu O 2010 Development of an MR-compatible SPECT system (MRSPECT) for simultaneous data acquisition *Phys. Med. Biol.* **55** 1563–75

Hartsough N E, Iwanczyk J S, Nygard E, Malakhov N, Barber W C and Gandhi T 2009 Polycrystalline mercuric iodide films on CMOS readout arrays *IEEE Trans. Nucl. Sci.* **56** 1810–6

Hazumi M 1996 BELLE silicon vertex detector *Nucl. Instrum. Methods Phys. Res.* A **379** 390–2

He Z, Li W, Knoll G F, Wehe D K, Berry J and Stahle C M 1999 3-D position sensitive CdZnTe gamma-ray spectrometers *Nucl. Instrum. Meth.* A **422** 173–8

Heemskerk J W, Korevaar M A, Huizenga J, Kreuger R, Schaart D R, Goorden M C and Beekman F J 2010 An enhanced high-resolution EMCCD-based gamma camera using SiPM side detection *Phys. Med. Biol.* **55** 6773–84

Heemskerk J W, Korevaar M A, Kreuger R, Ligtvoet C M, Schotanus P and Beekman F J 2009 A micro-machined retro-reflector for improving light yield in ultra-high-resolution gamma cameras *Phys. Med. Biol.* **54** 3003–14

Heemskerk J W, Westra A H, Linotte P M, Ligtvoet K M, Zbijewski W and Beekman F J 2007 Front-illuminated versus back-illuminated photon-counting CCD-based gamma camera: important consequences for spatial resolution and energy resolution *Phys. Med. Biol.* **52** N149–62

Herbert D J, Saveliev V, Belcari N, D'Ascenzo N, Del Guerra A and Golovin A 2006 First results of scintillator readout with silicon photomultiplier *IEEE Trans. Nucl. Sci.* **53** 389–94

Hesterman J Y, Caucci L, Kupinski M A, Barrett H H and Furenlid L R 2010 Maximum-likelihood estimation with a contracting-grid search algorithm *IEEE Trans. Nucl. Sci.* **57** 1077–84

Hofstadter R 1949 The detection of gamma-rays with thallium-activated sodium iodide crystals *Phys. Rev.* **75** 796

Hruska C B and O'Connor M K 2006 CZT detectors: How important is energy resolution for nuclear breast imaging? *Phys. Med.* **21** (Suppl. 1) 72–5

Hruska C B and O'Connor M K 2008 A Monte Carlo model for energy spectra analysis in dedicated nuclear breast imaging *IEEE Trans. Nucl. Sci.* **55** 491–500

Huber J S, Moses W W, Jones W F and Watson C C 2002 Effect of 176 Lu background on singles transmission for LSO-based PET cameras *Phys. Med. Biol.* **47** 3535

Hunter W, Barrett H H and Furenlid L R 2009 Calibration method for ML estimation of 3D interaction position in a thick gamma-ray detector *IEEE Trans. Nucl. Sci.* **56** 189–96

Hynecek J 1992 Theoretical analysis and optimization of CDS signal processing method for CCD image sensors *IEEE Trans. Electron Devices* **39** 2497–507

Ichihara T, Ogawa K, Motomura N, Kubo A and Hashimoto S 1993 Compton scatter compensation using the triple-energy window method for single- and dual-isotope SPECT *J. Nucl. Med.* **34** 2216–21

Jerram P, Pool P J, Bell R, Burt D J, Bowring S, Spencer S, Hazelwood M, Moody I, Catlett N and Heyes P S 2001 *The LLCCD: Low-light Imaging without the Need for an Intensifier* ed M M Blouke *et al* (San Jose, CA: SPIE) pp 178–86

Jia-Wei T, Liang C and Ling-Jian M 2009 A prototype of the MRI-compatible ultra-high resolution SPECT for *in vivo* mice brain imaging *Nuclear Science Symp. Conf. Record, 2009 IEEE* pp 2800–5

Johnson L C, Campbell D L, Hull E L and Peterson T E 2011 Characterization of a high-purity germanium detector for small-animal SPECT *Phys. Med. Biol.* accepted for publication

Kapusta M, Lavoute P, Lherbet F, Rossignol E, Moussant C and Fouche F 2007 Breakthrough in quantum efficiency of bi-alkali photocathodes PMTs *Nuclear Science Symp. Conf. Record, 2007 IEEE* pp 73–7

Kim H, Furenlid L R, Crawford M J, Wilson D W, Barber H B, Peterson T E, Hunter W C, Liu Z, Woolfenden J M and Barrett H H 2006 SemiSPECT: a small-animal single-photon emission computed tomography (SPECT) imager based on eight cadmium zinc telluride (CZT) detector arrays *Med. Phys.* **33** 465–74

Kopelman D, Blevis I, Iosilevsky G, Reznik A, Chaikov A, Weiner N, Israel O and Hashmonai M 2005 A newly developed intra-operative gamma camera: performance characteristics in a laboratory phantom study *Eur. J. Nucl. Med. Mol. Imaging* **32** 1217–24

Korevaar M A, Heemskerk J W and Beekman F J 2009a A pinhole gamma camera with optical depth-of-interaction elimination *Phys. Med. Biol.* **54** N267–N72

Korevaar M A, Heemskerk J W, Goorden M C and Beekman F J 2009b Multi-scale algorithm for improved scintillation detection in a CCD-based gamma camera *Phys. Med. Biol.* **54** 831–42

Kume H, Muramatsu S and Iida M 1986 Position sensitive photomultiplier tubes for scintillation imaging *IEEE Trans. Nucl. Sci.* **33** 359–63

Kung M P and Kung H F 2005 Mass effect of injected dose in small rodent imaging by SPECT and PET *Nucl. Med. Biol.* **32** 673–8

Kyushima H, Shimoi H, Atsumi A, Ito M, Oba K and Yoshizawa Y 2000 The development of flat panel PMT *Nuclear Science Symp. Conf. Record, 2000 IEEE* vol 1 pp 7/3–7

Levi A, Roth M, Schieber M, Lavy S and Cooper G 1982 The development of mercuric iodide gamma-radiation detectors for application in nuclear medicine *IEEE Trans. Nucl. Sci.* **29** 457–60

Links J M 1996 Simultaneous dual-radionuclide imaging: are the images trustworthy? *Eur. J. Nucl. Med. Mol. Imaging* **23** 1289–91

Llopart X, Campbell M, Dinapoli R, San Segundo D and Pernigotti E 2002 Medipix2: A 64-k pixel readout chip with 55 μm square elements working in single photon counting mode *IEEE Trans. Nucl. Sci.* **49** 2279–83

Luke P N, Amman M, Lee J S and Manfredi P F 2001 Noise in CdZnTe detectors *IEEE Trans. Nucl. Sci.* **48** 282–6

Luke P N, Amman M, Phlips B F, Johnson W N and Kroeger R A 2000 Germanium orthogonal strip detectors with amorphous-semiconductor contacts *IEEE Trans. Nucl. Sci.* **47** 1360–3

Luke P N and Eissler E E 1996 Performance of CdZnTe coplanar-grid gamma-ray detectors *IEEE Trans. Nucl. Sci.* **43** 1481–6

Macri J R, Hamel L A, Julien M, Miller R S, Donmez B, McConnell M L, Ryan J M and Widholm M 2004 Single-sided CZT strip detectors *IEEE Trans. Nucl. Sci.* **51** 2453–60

Madan S K, Bhaumik B and Vasi J M 1983 Experimental observation of avalanche multiplication in charge-coupled devices *IEEE Trans. Electron Devices* **30** 694–9

Madsen M T 2007 Recent advances in SPECT imaging *J. Nucl. Med.* **48** 661–73

Maehlum G, Dietzel K I, Meier D, Szawlowski M, Sundal B, Vandehei T, Wagenaar D and Patt B E 2007 Study of cadmium zinc telluride (CZT) radiation detector modules under moderate and long-term variations of temperature and humidity *Nuclear Science Symp. Conf. Record, 2007 IEEE* pp 1645–8

Mahmood S T, Erlandsson K, Cullum I and Hutton B F 2009 Design of a novel slit-slat collimator system for SPECT imaging of the human brain *Phys. Med. Biol.* **54** 3433–49

Marks D G, Barber H B, Barrett H H, Tueller J and Woolfenden J M 1999 Improving performance of a CdZnTe imaging array by mapping the detector with gamma rays *Nucl. Instrum. Methods Phys. Res.* A **428** 102–12

Marks D G *et al* 1996 A 48 × 48 CdZnTe array with multiplexer readout *IEEE Trans. Nucl. Sci.* **43** 1253–9

Marshall F-H, Coltman J W and Hunter L P 1947 The photomultiplier x-ray detector *Rev. Sci. Instrum.* **18** 504–13

Matherson K J, Barber H B, Barrett H H, Eskin J D, Dereniak E L, Marks D G, Woolfenden J M, Young E T and Augustine F L 1998 Progress in the development of large-area modular 64 × 64 CdZnTe imaging arrays for nuclear medicine *IEEE Trans. Nucl. Sci.* **45** 354–8

McElroy D P, Sung-Cheng H and Hoffman E J 2002 The use of retro-reflective tape for improving spatial resolution of scintillation detectors *IEEE Trans. Nucl. Sci.* **49** 165–71

Meier D *et al* 2002 Silicon detector for a Compton camera in nuclear medical imaging *IEEE Trans. Nucl. Sci.* **49** 812–6

Meikle S R, Kench P, Kassiou M and Banati R B 2005 Small animal SPECT and its place in the matrix of molecular imaging technologies *Phys. Med. Biol.* **50** R45–R61

Melcher C L and Schweitzer J S 1992 Cerium-doped lutetium oxyorthosilicate: a fast, efficient new scintillator *IEEE Trans. Nucl. Sci.* **39** 502–5

Meng L J 2006 An intensified EMCCD camera for low energy gamma ray imaging applications *IEEE Trans. Nucl. Sci.* **53** 2376–84

Meng L J, Tan J W, Spartiotis K and Schulman T 2009 Preliminary evaluation of a novel energy-resolved photon-counting gamma ray detector *Nucl. Instrum. Methods Phys. Res.* A **604** 548–54

Mettler F A *et al* 2009 Radiologic and nuclear medicine studies in the United States and worldwide: frequency, radiation dose, and comparison with other radiation sources—1950–20071 *Radiology* **253** 520–31

Miller B W, Barber H B, Furenlid L R, Moore S K and Barrett H H 2009a Progress of BazookaSPECT *Proc. SPIE* **7450** 74500C

Miller B W, Barrett H H, Furenlid L R, Barber H B and Hunter R J 2008 Recent advances in BazookaSPECT: real-time data processing and the development of a gamma-ray microscope *Nucl. Instrum. Methods Phys. Res.* **591** 272–5

Miller B W, Furenlid L R, Moore S K, Barber H B, Nagarkar V V and Barrett H H 2009b System integration of FastSPECT III, a dedicated SPECT rodent-brain imager based on BazookaSPECT detector technology *Nuclear Science Symp. Conf. Record, 2009 IEEE* pp 4004–8

Milster T D, Aarsvold J N, Barrett H H, Landesman A L, Mar L S, Patton D D, Roney T J, Rowe R K and Seacat R H 3rd 1990 A full-field modular gamma camera *J. Nucl. Med.* **31** 632–9

Moses W W 2002 Current trends in scintillator detectors and materials *Nucl. Instrum. Methods Phys. Res.* A **487** 123–8

Muehllehner G 1985 Effect of resolution improvement on required count density in ECT imaging: a computer simulation *Phys. Med. Biol.* **30** 163–73

Mueller B, O'Connor M K, Blevis I, Rhodes D J, Smith R, Collins D A and Phillips S W 2003 Evaluation of a small cadmium zinc telluride detector for scintimammography *J. Nucl. Med.* **44** 602–9

Nagarkar V V, Gupta T K, Miller S R, Klugerman Y, Squillante M R and Entine G 1998 Structured CsI(Tl) scintillators for X-ray imaging applications *IEEE Trans. Nucl. Sci.* **45** 492–6

Nagarkar V V, Shestakova I, Gaysinskiy V, Tipnis S V, Singh B, Barber W, Hasegawa B and Entine G 2006 A CCD-based detector for SPECT *IEEE Trans. Nucl. Sci.* **53** 54–8

Niraula M, Nakamura A, Aoki T, Tomita Y and Hatanaka Y 2002 Stability issues of high-energy resolution diode type CdTe nuclear radiation detectors in a long-term operation *Nucl. Instrum. Methods Phys. Res.* A **491** 168–75

O'Connor M K, Phillips S W, Hruska C B, Rhodes D J and Collins D A 2007 Molecular breast imaging: advantages and limitations of a scintimammographic technique in patients with small breast tumors *Breast J.* **13** 3–11

O'Connor M K, Wagenaar D, Hruska C B, Phillips S, Caravaglia G and Rhodes D 2006 Molecular breast imaging using a dedicated high-performance instrument *Proc. SPIE* **6319** 63191D

Ogawa K and Muraishi M 2010 Feasibility study on an ultra-high-resolution SPECT with CdTe detectors *IEEE Trans. Nucl. Sci.* **57** 17–24

Ogawa K, Ohmura N, Iida H, Nakamura K, Nakahara T and Kubo A 2009 Development of an ultra-high resolution SPECT system with a CdTe semiconductor detector *Ann. Nucl. Med.* **23** 763–70

Ozaktas H M and Urey H 1993 Space bandwidth product of conventional Fourier transforming systems *Opt. Commun.* **104** 29–31

Pangaud P, Basolo S, Boudet N, Berar J-F, Chantepie B, Delpierre P, Dinkespiler B, Hustache S, Menouni M and Morel C 2007 XPAD3: a new photon counting chip for x-ray CT-scanner *Nucl. Instrum. Methods Phys. Res.* A **571** 321–4

Pani R *et al* 2006 Lanthanum scintillation crystals for gamma ray imaging *Nucl. Instrum. Methods Phys. Res.* A **567** 294–7

Pani R, Scopinaro F, Pellegrini R, Soluri A, Weinberg I N and De Vincentis G 1997 The role of Compton background and breast compression on cancer detection in scintimammography *Anticancer Res.* **17** 1645–9

Parnham K B, Chowdhury S, Li J, Wagenaar D J and Patt B E 2006 Second-generation, tri-modality pre-clinical imaging system *Nuclear Science Symp. Conf. Record, 2006 IEEE* pp 1802–5

Patt B E, Beyerle A G, Dolin R C and Ortale C 1989 Developments in mercuric iodide gamma ray imaging *Nucl. Instrum. Methods Phys. Res.* A **283** 215–9

Patton D D 2000 The father of nuclear medicine: establishing paternity *J. Nucl. Med.* **41** 26N, 29N–30

Patton D D 2003 The birth of nuclear medicine instrumentation: Blumgart and Yens, 1925 *J. Nucl. Med.* **44** 1362–5

Payne S A, Cherepy N J, Hull G, Valentine J D, Moses W W and Woon-Seng C 2009 Nonproportionality of scintillator detectors: theory and experiment *IEEE Trans. Nucl. Sci.* **56** 2506–12

Peterson T E, Wilson D W and Barrett H H 2003 Application of silicon strip detectors to small-animal imaging *Nucl. Instrum. Meth.* A **505** 608–11

Petrillo M, Ye J, Vesel J, Shao L, Wieczorek H and Goedicke A 2004 Imaging performance of tiled solid-state detectors *Nuclear Science Symp. Conf. Record, 2004 IEEE* vol 4 pp 2306–12

Pettersen D M, Mikkelsen S, Talebi J and Meier D 2005 A readout ASIC for SPECT *IEEE Trans. Nucl. Sci.* **52** 764–71

Popov V, Majewski S and Weisenberger A G 2003 Readout electronics for multianode photomultiplier tubes with pad matrix anode layout *Nuclear Science Symp. Conf. Record, 2003 IEEE* vol 3 pp 2156–9

Radeka V 1988 Low-noise techniques in detectors *Annu. Rev. Nucl. Part. Sci.* **38** 217–77

Ramo S 1939 Currents induced by electron motion *Proc. Inst. Radio Eng.* **27** 584

Reddy B, Premachand K, Rao P and Parthasaradhi K 1992 Z-dependence of photoelectric cross-section in the energy region of absorption edges (6.4÷136.47) keV *Il Nuovo Cimento* A **105** 735–9

Robbins M S and Hadwen B J 2003 The noise performance of electron multiplying charge-coupled devices *IEEE Trans. Electron Devices* **50** 1227–32

Rogers W L, Clinthorne N H, Harkness B A, Koral K F and Keyes J W Jr 1982 Field-flood requirements for emission computed tomography with an Anger Camera *J. Nucl. Med.* **23** 162–8

Rogulski M M, Barber H B, Barrett H H, Shoemaker R L and Woolfenden J M 1993 Ultra-high-resolution brain SPECT imaging—simulation results *IEEE Trans. Nucl. Sci.* **40** 1123–9

Russo P, Mettivier G, Pani R, Pellegrini R, Cinti M N and Bennati P 2009 Imaging performance comparison between a LaBr3: Ce scintillator based and a CdTe semiconductor based photon counting compact gamma camera *Med. Phys.* **36** 1298–317

Rutao Y *et al* 2008 Lutetium oxyorthosilicate (LSO) intrinsic activity correction and minimal detectable target activity study for SPECT imaging with a LSO-based animal PET scanner *Phys. Med. Biol.* **53** 4399

Sanchez F *et al* 2006 Performance tests of two portable mini gamma cameras for medical applications *Med. Phys.* **33** 4210–20

Schieber M, Roth M and Schnepple W F 1983 Crystal growth and applications of mercuric iodide *J. Cryst. Growth* **65** 353–64

Schlomka J P *et al* 2008 Experimental feasibility of multi-energy photon-counting K-edge imaging in pre-clinical computed tomography *Phys. Med. Biol.* **53** 4031

Schmid G J, Beckedahl D A, Kammeraad J E, Blair J J, Vetter K and Kuhn A 2001 Gamma-ray Compton camera imaging with a segmented HPGe *Nucl. Instrum. Meth.* A **459** 565–76

Shah K S, Farrell R, Grazioso R, Harmon E S and Karplus E 2002 Position-sensitive avalanche photodiodes for gamma-ray imaging *IEEE Trans. Nucl. Sci.* **49** 1687–92

Shah K S, Farrell R, Grazioso R, Myers R and Cirignano L 2001 Large-area APDs and monolithic APD arrays *IEEE Trans. Nucl. Sci.* **48** 2352–6

Shah K S, Glodo J, Klugerman M, Moses W W, Derenzo S E and Weber M J 2003 $LaBr_3$:Ce scintillators for gamma-ray spectroscopy *IEEE Trans. Nucl. Sci.* **50** 2410–3

Shockley W 1938 Currents to conductors induced by a moving point charge *J. Appl. Phys.* **9** 635

Shokouhi S, McDonald B S, Durko H L, Fritz M A, Furenlid L R and Peterson T E 2009 Thick silicon double-sided strip detectors for low-energy small-animal SPECT *IEEE Trans. Nucl. Sci.* **56** 557–64

Siffert P, Berger J, Scharager C, Cornet A, Stuck R, Bell R O, Serreze H B and Wald F V 1976 Polarization in cadmium telluride nuclear radiation detectors *IEEE Trans. Nucl. Sci.* **23** 159–70

Soesbe T C, Lewis M A, Slavine N V, Richer E, Bonte F J and Antich P P 2010 High-resolution photon counting using a lens-coupled EMCCD gamma camera *IEEE Trans. Nucl. Sci.* **57** 958–63

Spagnoli L G, Bonanno E, Sangiorgi G and Mauriello A 2007 Role of inflammation in atherosclerosis *J. Nucl. Med.* **48** 1800–15

St James S, Yang Y, Wu Y, Farrell R, Dokhale P, Shah K S and Cherry S R 2009 Experimental characterization and system simulations of depth of interaction PET detectors using 0.5 mm and 0.7 mm LSO arrays *Phys. Med. Biol.* **54** 4605

Szeles C, Soldner S A, Vydrin S, Graves J and Bale D S 2008 CdZnTe semiconductor detectors for spectroscopic X-ray imaging *IEEE Trans. Nucl. Sci.* **55** 572–82

Tornai M P, Archer C N, Weisenberger A G, Wojcik R, Popov V, Majewski S, Keppel C E, Levin C S, Tipnis S V and Nagarkar V V 2001 Investigation of microcolumnar scintillators on an optical fiber coupled compact imaging system *IEEE Trans. Nucl. Sci.* **48** 637–44

Truman A, Bird A J, Ramsden D and He Z 1994 Pixellated CsI(T1) arrays with position-sensitive PMT readout *Nucl. Instrum. Methods Phys. Res.* A **353** 375–8

Tsuchimochi M, Hayama K, Oda T, Togashi M and Sakahara H 2008 Evaluation of the efficacy of a small CdTe γ-Camera for sentinel lymph node biopsy *J. Nucl. Med.* **49** 956–62

Tsui B M, Metz C E, Atkins F B, Starr S J and Beck R N 1978 A comparison of optimum detector spatial resolution in nuclear imaging based on statistical theory and on observer performance *Phys. Med. Biol.* **23** 654–76

Tsyganov E, Antich P, Parkey R, Seliounine S, Golovatyuk V, Lobastov S, Zhezher V and Buzulutskov A 2008 Gas electron multiplying detectors for medical applications *Nucl. Instrum. Methods Phys. Res.* A **597** 257–65

Vadawale S V, Purohit S, Shanmugam M, Acharya Y B, Goswami J N, Sudhakar M and Sreekumar P 2009 Characterization and selection of CZT detector modules for HEX experiment onboard Chandrayaan-1 *Nucl. Instrum. Methods Phys. Res.* A **598** 485–95

van Dam H T, Seifert S, Vinke R, Dendooven P, Löhner H, Beekman F J and Schaart D R 2010 A comprehensive model of the response of silicon photomultipliers *IEEE Trans. Nucl. Sci.* **57** 2254–66

van Eijk C W 2002 Inorganic scintillators in medical imaging *Phys. Med. Biol.* **47** R85–106

van Loef E V D, Dorenbos L P, van Eijk C W E, Kramer K and Gudel H U 2001 Scintillation properties of $LaCl_3$:Ce^{3+} crystals: fast, efficient, and high-energy resolution scintillators *IEEE Trans. Nucl. Sci.* **48** 341–5

Vermeeren L, Valdes Olmos R A, Klop W M C, Balm A J M and van den Brekel M W M 2010 A portable γ-Camera for intraoperative detection of sentinel nodes in the head and neck region *J. Nucl. Med.* **51** 700–3

Villena J L, Tapias G, Lage E, Kreuger R and Beekman F J 2010 Evaluation of a 25–511 keV list mode readout system for a large field-of-view gamma camera *Nuclear Science Symp. Conf. Record, 2010 IEEE* pp 2168–73

Volokh L, Hugg J, Blevis I, Asma E, Jansen F and Manjeshwar R 2008 Effect of detector energy response on image quality of myocardial perfusion SPECT *Nuclear Science Symp. Conf. Record, 2008 IEEE* pp 4043–6

Wagenaar D J, Chowdhury S, Engdahl J C and Burckhardt D D 2003 Planar image quality comparison between a CdZnTe prototype and a standard NaI(Tl) gamma camera *Nucl. Instrum. Methods Phys. Res.* A **505** 586–9

Weisenberger A G, Kross B, Majewski S, Wojlck R, Bradley E L and Saha M S 1998 Design features and performance of a CsI(Na) array based gamma camera for small animal gene research *IEEE Trans. Nucl. Sci.* **45** 3053–8

Weisenberger A G, Majewski S, Popov V and Wojcik R 2001 High resolution detector modules based on NaI(Tl) arrays for small animal imaging *Nuclear Science Symp. Conf. Record, 2001 IEEE* vol 3 pp 1540–4

Wernick M and Aarsvold J 2004 *Emission Tomography: The Fundamentals of PET and SPECT* (Amsterdam: Elsevier)

Williams M B, Williams M B, Goode A R, Galbis-Reig V, Majewski S, Weisenberger A G and Wojcik R 2000 Performance of a PSPMT based detector for scintimammography *Phys. Med. Biol.* **45** 781–800

Wong W H 1993 A positron camera detector design with cross-coupled scintillators and quadrant sharing photomultipliers *IEEE Trans. Nucl. Sci.* **40** 962–6

Xi W, Seidel J, Kakareka J W, Pohida T J, Milenic D E, Proffitt J, Majewski S, Weisenberger A G, Green M V and Choyke P L 2010 MONICA: a compact, portable dual gamma camera system for mouse whole-body imaging *Nucl. Med. Biol.* **37** 245–53

Zentai G, Schieber M, Partain L, Pavlyuchkova R and Proano C 2005 Large area mercuric iodide and lead iodide X-ray detectors for medical and non-destructive industrial imaging *J. Cryst. Growth* **275** e1327–e31

Zhang J, Olcott P D and Levin C S 2007 A new positioning algorithm for position-sensitive avalanche photodiodes *IEEE Trans. Nucl. Sci.* **54** 433–7